Comments from Anonymous Referee #1

Received and published: 21 November 2017

I think that the manuscript is excellent. I only suggest insert these further references, concerning the statistical models, at page 4 line 67-69:

Baum, R.L., and Godt, J.W. Early warning of rainfall-induced shallow landslides and debris flows in the USA, Landslides, 7(3), 259-272. DOI: 10.1007/s10346-009-0177-0, 2010.

Berti, M., Martina, M.L.V., Franceschini, S., Pignone, S., Simoni, A., and Pizziolo, M. Probabilistic rainfall thresholds for landslide occurrence using a Bayesian approach, Journal of Geophysical Research: Earth Surface, 117 (4), doi:10.1029/2012JF002367, 2012.

Cannon, S.H., Gartner, J.E., Wilson, R., Bowers, J., and Laber, J. Storm rainfall conditions for floods and debris flows from recently burned areas in southwestern Colorado and southern California, Geomorphology, 96(3–4), 250–269, DOI: 10.1016/j.geomorph.2007.03.019, 2008.

De Luca D.L.; Versace P. A comprehensive framework for empirical modeling of landslides induced by rainfall: the Generalized FLaIR Model (GFM). Landslides, 14(3): 1009-1030, ISSN: 1612-5118, DOI: 10.1007/s10346-016-0768-5, 2017.

Godt, J.W., Baum, R.L., and Chleborad, A.F. Rainfall characteristics for shallow landsliding in Seattle, Washington, USA. Earth Surface Processes and Landforms, 31, 97-110, DOI: 10.1002/esp.1237, 2006.

Guzzetti, F., Peruccacci, S., Rossi, M. and Stark, C.P. The rainfall intensity–duration control of shallow landslides and debris flows: An update, Landslides, 5, 3–17, DOI: 10.1007/s10346-007-0112-1, 2008.

Staley, D.M., Kean, J.W., Cannon, S.H., Schmidt, K.M., and Laber, J.L. Objective definition of rainfall intensity–duration thresholds for the initiation of post-fire debris flows in southern California, Landslides, 10(5), 547-562 DOI:10.1007/s10346-012-0341-9, 2013.

After addition of these references, in my opinion the manuscript is ready for publication**.**

Authors' Response

Thank you so much for the comments. Your suggestion is well taken and helpful to make the manuscript more informative and comprehensive. We have added the references you suggested.

Author's changes in manuscript

Lines 66-72: Statistical models have also been proposed to relate debris-flow initiation to rainfall (e.g. Caine, 1980; Wieczorek, 1987; Chen et al., 2005; Godt et al., 2006; Cannon et al., 2008; Coe et al., 2008; Guzzetti, et al., 2008; Baum and Godt, 2010; Berti et al., 2012; Staley et al., 2013; Zhou and Tang, 2014; De Luca and Versace, 2017a; De Luca and Versace, 2017b; Gao et al., 2017) and other parameters such as surface runoff discharge (Berti and Simoni, 2005) or clay content (Chen et al., 2010).

Comments from Anonymous Referee #2

Received and published: 20 March 2018

Version 2.0 of the EDDA model features improvements over the previous version. However, its process representation is still deterministically-derived, and it rests on assumptions that limit the veracity of the physics-based representations of key processes. Some examples: Line 189 - the assumption here is that surface runoff is generated solely by Hortonian Overland Flow - that is the rainfall intensity exceeds the infiltration capacity. In fact, surface runoff is often associated with other situations and locations. Saturation Overland Flow (SOF) is another likely driver of surface erosion that may trigger a debris flow, for example. The spatial distribution of SOF is largely, topographically controlled and could be predicted based on the DEM and application of appropriate topographic analyses. Line 197 - Richards equation is outmoded. We know it doesn't work. It should be replaced in EDDA 3.0 by a current approach to simulating through flow. Line 214 - Terrain places an important role in determining the initiation point and pathway for a debris flow. This is not well represented by the infinite slope model. Line 245 - the du Boys shear stress equation is old and outmoded. There are better methods based on, for example, specific stream power (stream power per unit bed area). Goodness of fit - describing model and observed results as agreeing 'reasonably well' is insufficient. Quantitative criteria for agreement should be derived and applied to test 'goodness of fit'. Notwithstanding these criticisms, the model and paper have merit and can be used for broad scale forecasting of debris flows triggered by rainfall that is heavy and/or prolonged.

Authors' Response

Thank you so much for the constructive and helpful comments. The response to your comments is as follow.

1. "Line 189 - the assumption here is that surface runoff is generated solely by Hortonian Overland Flow - that is the rainfall intensity exceeds the infiltration capacity. In fact, surface runoff is often associated with other situations and locations. Saturation Overland Flow (SOF) is another likely driver of surface erosion that may trigger a debris flow, for example. The spatial distribution of SOF is largely, topographically controlled and could be predicted based on the DEM and application of appropriate topographic analyses."

Indeed the Hortonian runoff concept cannot explain storm runoff in many of the humid regions where the infiltration capacity of the ground is typically much greater than average rainfall intensities. Steenhuis and Muck (1988) found that soils of the Ithaca NY, especially the shallow hillside soils maintained in grass and pasture, have infiltration rates that are rarely exceeded by the rainfall rate. This has been confirmed in other studies (Merwin et al., 1994; Dunne and Black, 1970). For example, over 90% of the soils in Delaware County, NY (in the Catskill Mountains) have permeabilities above 3 cm/hr. However, rainfall intensities greater than 3 cm/hr are rare. In contrast, storm responses in streams reflect runoff processes occurring upstream almost every time it rains, which means that there must be some mechanisms other than Hortonian Flow that generate runoff. Since then, researchers have found other runoff-generating mechanisms, such as saturation overland flow (SOF).

The SOF has two sources, Direct Precipitation onto Saturated Areas (DPSA) and Return Flow (RF). Rain falling on already-saturated soil has no option but to run off. This case is termed direct precipitation on saturated areas (DPSA). The return flow (RF) occurs if the rate of interflow entering a saturated area from upslope exceeds the capacity for interflow to leave the area by flowing downhill through the soil. The excess interflow thus "returns" to the surface as runoff. The combination of RF and DPS is called saturation overland flow.

This mechanism derives a concept called Variable Source Area (VSA) which recognizes that the extent of saturated areas in a watershed will vary temporally. Before a storm, saturated areas are limited to the close vicinity of the stream. They expand during the storm, resulting in a larger rate of runoff generation. The application of this concept utilizes the information including bedrock, impermeable soil layers, and/or the depth to the water table. Thus, both hydrologic and soil-water concepts are combined to evaluate potential runoff areas in the landscape.

In this paper, the debris flow case being simulated occurred in the Wenchuan earthquake zone. A large part of the study area remained uncovered by vegetation before the debris flow event, because the Wenchuan earthquake triggered many landslides and the previous vegetation cover was wiped out. Also considering that the fresh landslide deposits had a relative fine-grained surface, which is due to an inverse segregation mechanism, infiltration capacity becomes a limiting factor in this study and Hortonian overland flow is thus a dominant process.

Your suggestion is very good and appreciated. We will revise/expand the runoff mechanisms in the model in the future version to make the model more comprehensive.

References

[1] Dunne T and Black RD (1970) Partial area contributions to storm runoff in a small New England watershed. Water Resources Research 6(5): 1296-1311.

[2] Merwin IA, Stiles WC and van Es HM (1994) Orchard groundcover management impacts on soil physical properties. Journal of the American Society for Horticultural Science 119(2): 216-222.

[3] Steenhuis TS and Muck RE (1988) Preferred movement of nonadsorbed chemicals on wet, shallow, sloping soils. Journal of Environmental Quality 17(3): 376-384.

2. "Line 197 - Richards equation is outmoded. we know it doesn't work. It should be replaced in EDDA 3.0 by a current approach to simulating through flow."

Zhang et al. (2011) made a comprehensive review of existing research on infiltration analysis. Based on this review, there are two main types of infiltration analysis methods.

(1) Conceptual infiltration models. Infiltration models have been proposed based on a wetting front concept (Green and Ampt, 1911; Lumb, 1962; Mein and Larson, 1973; Sun et al., 1998). However, serious limitations impose restrictions on the use of the conceptual infiltration models, because they usually do not consider sloping ground conditions, down-slope flows, variation of rainfall intensity or, most importantly, the dependence of soil permeability on moisture content (Ng and Shi, 1998b). In addition, there may not be a distinct difference between the infiltration zone and the unsaturated zone.

(2) Analytical and numerical solutions. A combination of Darcy's law as applied to unsaturated flow and the equation of continuity is considered the most robust method available for computing infiltration and soil moisture profiles in saturated–unsaturated soil systems. Based on Darcy's law and the mass conservation for water flow, the three-dimensional water flow in unsaturated soil is described by the Richards equation (Richards, 1931; Fredlund and Rahardjo, 1993). Many analytical solutions (e.g., Srivastava and Yeh, 1991; Iverson, 2000; Chen et al.,

2001; Yuan and Lu, 2005), numerical solutions (e.g., Ng and Shi, 1998a; Gasmo et al., 2000; Tsaparas et al., 2002; Blatz et al., 2004; Zhang et al., 2004; Rahardjo et al., 2007; Rahimi et al., 2010) and computer programs (e.g., Seep/W (Geo-slope Ltd, 2001); SVflux (SoilVision System Ltd, 2001); Flow3D (Gerscovich, 1994); and FEMWATER (Lin et al., 1997)) have been proposed for solving the Richards equation. However, analytical solutions for the infiltration problem can be obtained only by making some assumptions, and under some given initial and boundary conditions because of the natural spatial variability in the field, uncertain initial conditions and boundary conditions, and complex soil layering in practical applications.

Another theory for modeling the seepage process is the computational fluid dynamics/discrete element method (CFD-DEM model). However, this method is computationally demanding and may not be applicable to catchment-scale studies.

We are very interested in latest methods for simulating through flow and will study and adopt one in the future version of EDDA.

Reference

[1] Blatz JA, Ferreira NJ and Graham J (2004) Effects of near-surface environmental conditions on instability of an unsaturated soil slope. Canadian Geotechnical Journal 41(6): 1111-1126.

[2] Chen JM, Tan YC and Chen CH (2001) Multidimensional infiltration with arbitrary surface fluxes. Journal of Irrigation and Drainage Engineering, ASCE 127(6): 370-377.

[3] Fredlund DG and Rahardjo H (1993) Soil Mechanics for Unsaturated Soils. Wiley, New York, NY, USA.

[4] Gasmo JM, Rahardjo H and Leong EC (2000) Infiltration effects on stability of a residual soil slope. Computers and Geotechnics 26(2): 145-165.

[5] Geo-slope Ltd (2001) Seep/W for Finite Element Seepage Analysis: User's Guide. Geo-Slope Ltd, Calgary, Canada.

[6] Gerscovich DMS (1994) Flow Through Saturated-Unsaturated Porous Media: Numerical Modelling and Slope Stability Studies of Rio de Janeiro Natural Slopes. PhD thesis, Catholic University of Rio de Janeiro, Brazil.

[7] Green WH and Ampt CA (1911) Studies on soil physics: flow of air and water through soils. Journal of Agricultural Science 4: 1-24.

[8] Iverson RM (2000) Landslide triggering by rain infiltration. Water Resources Research 36(7): 1897-1910.

[9] Lin HC, Richards DR, Talbot CA, Yeh GT, Cheng JR, Cheng HP and Jones NL (1997) Femwater: A Three-Dimensional Finite Element Computer Model for Simulation of Density-Dependent Flow and Transport in Variably Saturated Media. United States Waterways Experiment Station, Coastal and Hydraulics Laboratory, Vicksburg, MS, USA, Technical Report CHl-97-12.

[10] Lumb P (1962) Effect of rain storms on slope stability. Proceedings of the symposium on Hong Kong Soils, Hong Kong, pp. 73-87.

[11] Mein RG and Larson CL (1973) Modelling infiltration during a steady rain. Water Resources Research 9(2): 384-394.

[12] Ng CWW and Shi Q (1998a) Influence of rainfall intensity and duration on slope stability in unsaturated soils. Quarterly Journal of Engineering Geology 31(2): 105-113.

[13] Ng CWW and Shi Q (1998b) Numerical investigation of the stability of unsaturated soil slopes subjected to transient seepage. Computers and Geotechnics 22(1): 1-28.

[14] Rahardjo H, Ong TH, Rezaur RB and Leong EC (2007) Factors controlling instability of homogeneous soil slopes under rainfall. Journal of Geotechnical and Geoenvironmental Engineering 133(12): 1532-1543.

[15] Rahimi A, Rahardjo H and Leong EC (2010) Effect of hydraulic properties of soil on rainfall-induced slope failure. Engineering Geology 114(3-4): 135-143.

[16] Richards LA (1931) Capillary conduction of liquids through porous mediums. Physics 1: 318-333.

[17] Srivastava R and Yeh TCJ (1991) Analytical solutions for one-dimension transient infiltration toward the water table in homogeneous and layered soils. Water Resources Research 27(5): 753-762.

[18] Sun HW, Wong HN and Ho KKS (1998) Analysis of infiltration in unsaturated ground. In Slope Engineering in Hong Kong (Li KS, Kay JN and Ho KKS (eds)). Balkema, Rotterdam, the Netherlands, pp. 101-109.

[19] Tsaparas I, Rahardjo H, Toll DG and Leong EC (2002) Controlling parameters for rainfall-induced landslides. Computers and Geotechnics 29(1): 1-27.

[20] Yuan FS and Lu ZM (2005) Analytical solutions for vertical flow in unsaturated, rooted soils with variable surface fluxes. Vadose Zone Journal 4(4): 1210-1218.

[21] Zhang LL, Fredlund DG, Zhang LM and Tang WH (2004) Numerical study of soil conditions under which matric suction can be maintained. Canadian Geotechnical Journal 41(4): 569-582.

[22] Zhang LL, Zhang J, Zhang LM and Tang WH (2011) Stability analysis of rainfall-induced slope failure: a review. Proceedings of the Institution of Civil Engineers Geotechnical Engineering, 164(5), 299-316.

3. "Line 214 - Terrain places an important role in determining the initiation point and pathway for a debris flow. This is not well represented by the infinite slope model."

In this study, rain-induced landslide is one of the initiation mechanisms. These landslides are normally shallow, with a depth of failure less than 3 m, and generally of small volume on steep soil slopes of 30-50° (Dai et al., 2003; Johnson and Sitar, 1990). Considering that these rain-induced landslides are shallow-seated, the thickness of the sliding mass is small compared to the large plan dimensions of these slopes. Therefore, an infinite slope model for two-layer soil slopes is a reasonable option to evaluate the slope stability. The terrain is not treated as an infinitely straight surface. In fact, the terrain is discretized into cells based on the real topographic conditions. Each cell has different sloping gradient and is evaluated using the infinite model. The infinite slope model is a simplified method to achieve a balance between accuracy and computational time for catchment scale studies.

The traveling process of debris flow is simulated using mass conservation and momentum equations. The effects of terrain are involved in the equations. So, the debris flow is simulated to march along an optimal (the steepest) pathway automatically, based on the given terrain data.

4. "Line 245 - the du Boys shear stress equation is old and outmoded. There are better methods based on, for example, specific stream power (stream power per unit bed area)."

Thank you very much for your suggestions. There are erosion models based on the perspective of energy, which is widely used in hydrological studies. As Bagnold (1977) commented, since stream power and sediment transport rate are different values of the same physical quantity, it is rationale to relate one to the other. This is a heuristic enlightenment for us to consider interdisciplinary research in the future. The method of stream power is mainly used for sediment entrainment and transportation in a river system where clear water flow dominates the process. Before adopting relevant models, it is critical to evaluate whether and how these models can be used to describe the material entrainment by earth-surface mass flows that have very high solid-phase concentration. Besides, there is limited research on calibrating the threshold specific stream power of the ravines like the study area in this paper. Considering all of these issues, we regard them as good potential areas to be tacked, perhaps in EDDA3.0 as mentioned in your comments. We are interested in these problems and will work on them when developing the future version of the proposed model.

Reference

[1] Bagnold RA (1977) Bed Load Transport by Natural Rivers. Water Resource Research 13(2): 303-312.

5. "Goodness of fit - describing model and observed results as agreeing 'reasonably well' is insufficient. Quantitative criteria for agreement should be derived and applied to test 'goodness of fit'."

(1) Line 366 - "It is found that the results of the two separate analyses are very similar. The computed total scar area is 4.42×10^5 m^2, comparing well with 5.20×10^5 m^2 from the satellite image. It is concluded that the proposed slope stability module performs reasonably well."

The distribution of the computed unstable cell has been verified by Chen and Zhang (2014) using the confusing matrix method, shown in Figure 1. The results indicate that the proposed model is

capable of predicting the locations of rainfall-induced landslides reasonably well. For brevity, we omitted the presentation of the quantitative analysis of the degree of coincidence.

The computed total area of landslides is 4.42×10^5 m^2 and the observed value is 5.20×10^5 m^2. The difference is about 15%, which may be acceptable for large-scale numerical simulations. We will add this to the revised manuscript.

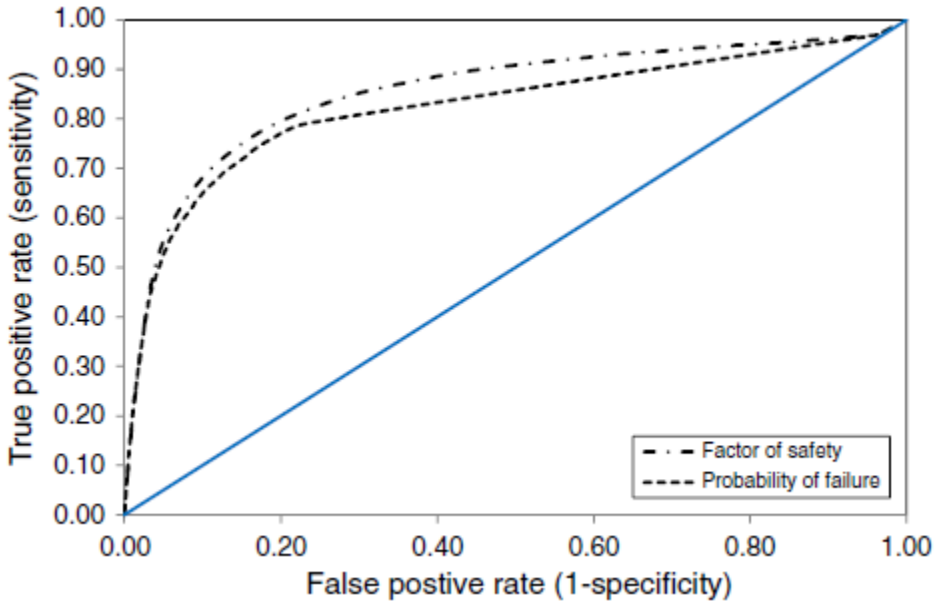

Figure 1. Receiver Operating Characteristic (ROC) curves in the form of factor of safety and probability of failure at the end of storm. The true positive rate (TPR) is the ratio of TP to (TP + FN); the false positive rate is the ratio of FP to (FP + TN).

(2) Line 414 - "The simulated and observed deposition areas are compared in Fig. 11. It is seen that the simulation results (Fig. 11a) match the observation (Fig. 11b) reasonably well. The simulated deposition depth is approximately 20 m, very close to that of the observed thickness of the deposit fan during the field investigations. The total volume of the observed deposition fan is about 1.17×10^6 m^3, while the simulated deposition volume of the debris flow is 0.9×10^6 m^3. The integrated model evaluates a smaller debris flow volume. The main uncertainty arises from the slope failure module and surface erosion module."

The simulated deposition volume (0.9×10^6 m^3) and the observed volume (1.17×10^6 m^3) differ by about 23%, which is also acceptable for numerical simulations, considering inevitable uncertainties such as spatial variability along a large distance. We will add this to the revised manuscript. However, such comparison is still rather qualitative. Numerical simulation of large-scale debris flows is still a challenge.

Author's changes in manuscript

1. Lines 362-366: Moreover, the results are compared with those by Chen and Zhang (2014), which have been verified using the confusing matrix method (e.g. Van Den Eeckhaut et al., 2006). It is found that the results of the two separate analyses are very similar. The computed total scar area is 4.42×10^5 m^2, comparing well with 5.20×10^5 m^2 from the satellite image. The difference is 15%. It is concluded that the proposed slope stability module performs reasonably well.

2. Lines 413-419: The simulated and observed deposition areas are compared in Fig. 11. It is seen that the simulation results (Fig. 11a) match the observations (Fig. 11b) reasonably well. The simulated deposition depth is approximately 20 m, very close to that of the observed thickness of the deposit fan during the field investigations. The total volume of the observed deposition fan is about 1.17×10^6 m^3, while the simulated deposition volume of the debris flow is 0.9×10^6 m^3. The integrated model evaluates a smaller debris flow volume and the difference is 23%. The main uncertainty arises from errors in the slope failure module and the surface erosion module.

EDDA 2.0: integrated simulation of debris flow initiation and dynamics, considering two initiation mechanisms

Ping Shen[a], Limin Zhang[a] *, Hongxin Chen[b], Ruilin Fan[a]

* Corresponding author.

Email address: pshen@connect.ust.hk (P. Shen), cezhangl@ust.hk (L. M. Zhang), chenhongxin@tongji.edu.cn (H. X. Chen), rfanaa@connect.ust.hk (R. L. Fan)

[a] Department of Civil and Environmental Engineering, The Hong Kong University of Science and Technology, Clear Water Bay, Hong Kong

[b] Key Laboratory of Geotechnical and Underground Engineering of Ministry of Education, Department of Geotechnical Engineering, Tongji University, China.

Abstract: Climate change results in more frequent rainstorms and more rain-induced debris flows in mountainous areas. The prediction of likely hazard zones is important for debris flow risk assessment and management. Existing numerical methods for debris flow analysis often require the input of hydrographs at prescribed initiation locations, ignoring the initiation process and leading to large uncertainties in debris flow initiation locations, times and volumes when applied to regional debris flow analysis. The evolution of the flowing mixture in time and space is hardly addressed either. This paper presents a new integrated numerical model, EDDA 2.0, to simulate the whole process of debris-flow initiation, motion, entrainment, deposition and property changes. Two physical initiation mechanisms are modeled: transformation from slope failures and surface erosion. Three numerical tests and field application to a catastrophic debris flow event are conducted to verify the model components and evaluate the model performance. The results indicate that the integrated model is capable of simulating the initiation and subsequent flowing process of rain-induced debris flows, as well as the physical evolution of the flowing mixture. The integrated model provides a powerful tool for analyzing multi-hazard processes, hazard interactions and regional debris-flow risk assessment in the future.

Keywords: debris flow; numerical modeling; rainfall infiltration; slope stability; erosion; entrainment.

1 Introduction

Debris flows are one of the most catastrophic hazards in mountainous areas (e.g. Zhang et al., 2013; Raia et al., 2014), and can pose high risks to society (e.g. Tang et al., 2011; Gao et al., 2016). They are often triggered by heavy rainfall and sensitive to climate change (e.g. Wong, 2009; Lee et al., 2010). As extreme rainstorms become more frequent, coping with rain-induced debris flows thus becomes critical in debris-flow prone regions such as Italy, Japan, Hong Kong and earthquake-affected areas in Sichuan, China.

During a storm, debris flows may be initiated by surface erosion, slope failures or dam breaching (e.g. Takahashi, 2007), and enlarged during the subsequent flowing process (e.g. Iverson, 1997). The debris flow mixture finally deposits in a flatter area, while the interstice fluid still flows along the debris flow track without further material entrainment as rainfall continues. The evolution of the flowing mixture includes three phases in terms of sediment concentration: clear water flow, hyperconcentrated flow and debris flow. The transition of the flowing mixture between any two phases occurs spatially and temporally during the whole process of rainfall.

Many numerical programs have been successfully developed for debris flow analysis, such as DAMBRK (Boss Corporation 1989), FLO-2D (O'Brien et al. 1993), DAN (Hungr 1995), DMM (Kwan and Sun 2006), Debris2D (Liu and Huang 2006), FLATModel (Medina et al. 2008), MassMov2D (Beguería et al. 2009), DAN3D (Hungr and McDougall 2009), PASTOR (Pastor et al. 2009), RAMMS (Bartelt et al., 2013), EDDA 1.0 (Chen and Zhang 2015), DebrisInterMixing (Boetticher et al., 2016) and AschFlow (Quan Luna et al., 2016). These programs can simulate the debris-flow movement with either constant or varying properties of the flowing mixture. The entrainment and deposition processes can also be considered, such as in EDDA 1.0 (Chen and Zhang, 2015).

Until now, numerical simulation of the physical process of debris flow initiation is

largely avoided in the literature. Moreover, very limited attempt has been made to simulate, in an integrated manner, the entire process from the initiation to the subsequent debris-flow motion and deposition. We address these two research gaps in this paper.

Experimental studies and field monitoring have been conducted to study the initiation mechanics of rain-induced debris flows (e.g. Johnson and Sitar, 1990; Cui, 1992; Cannon et al., 2001). A few physical models have been proposed (e.g. Takahashi, 1981; Iverson et al., 1997) to reveal the mechanisms of initiation using infinite slope stability models which are mathematically one-dimensional and statically determinate, leading to unambiguous quantitative results. However, these models do not simulate the debris-flow initiation process, particularly the transformation from a slope failure to a debris flow. Statistical models have also been proposed to relate debris-flow initiation to rainfall (e.g. Caine, 1980; Wieczorek, 1987; Chen et al., 2005; Godt et al., 2006; Cannon et al., 2008; Coe et al., 2008; Guzzetti, et al., 2008; Baum and Godt, 2010; Berti et al., 2012; Staley et al., 2013; Zhou and Tang, 2014; De Luca and Versace, 2017a; De Luca and Versace, 2017b; Gao et al., 2017) and other parameters such as surface runoff discharge (Berti and Simoni, 2005) or clay content (Chen et al., 2010). These models are not physically-based.

Many of the existing computer programs do not simulate the initiation of debris flows. Instead, they require a predefined empirical hydrograph, created based on the estimated volumes of rainfall runoff and source materials, to initiate a debris flow, which is so called "two-step" analysis (Fig. 1). The "two-step" analysis leads to large uncertainties in debris flow initiation locations, times and volumes when applied to regional debris flow analysis. For instance, Shen et al. (2017) simulated hillslope debris flows initiated from surface erosion, in which the initiation location is artificially intervened (Fig. 1), and the slope failure mechanisms is not included. The integrated simulation of the whole process of the debris flow (Fig. 1) remains an open challenge. In addition, the physical rainfall runoff and overland

flow process before the initiation of debris flows is overlooked. Until now, the study on the full evolution in time and space of the flowing mixture is limited.

Numerical tools have been generally developed for simulating a single type of hazards. However, multiple types of hazards may be induced by a rainstorm (i.e. slope failures, debris flows and flooding) (e.g. Zhang et al., 2014). One hazard can be the cause of another (e.g. rainfall triggers slope failures that in turn trigger debris flows). Different types of hazards can also interact among each other (e.g. several small debris flows from sub-channels can merger into a larger one). Hazard risk assessment requires hydrological, landslide and debris flow analyses at a regional scale (e.g. Formetta et al., 2011; Archfield et al., 2013). The simulation of the complete processes of possible hazards and their interactions at a regional scale can be a powerful tool to help identify likely hazards, their potentially affected areas and elements at risk. However, the ability of numerical analysis of hazard interactions is still limited (e.g. Kappes et al., 2012; Marzocchi et al., 2012). Using the existing “two-step” tools (Fig. 1) to analyze potential regional hazards could be challenging, since it involves tremendous uncertainties and is time-consuming to conduct the “two-step” analyses for each of all potential hazard locations (e.g. Chen and Zhang, 2015; Gao et al., 2016; Shen et al, 2017). Hence the development of an integrated model for simulating multi-hazard processes and interactions (Fig. 1) is of great theoretical and practical importance.

The objectives of this paper are (1) to incorporate debris-flow initiation physically into the debris-flow motion simulation to enable the simulation of the whole process of rain-induced debris flows, (2) to study the full evolution of the flowing mixture in time and space during the whole process of rainfall, and (3) to develop a tool to simulate multi-hazard processes and analyze hazard interactions.

2 Methodology

2.1 Strategy of modeling initiation, dynamics and deposition of debris flows

Intense rainfall in mountainous regions could trigger debris flows from loose soil deposits on hill slopes or in channels. A conceptual model for rain-induced debris flows and likely initiation mechanisms are shown in Fig. 2. Debris flows can be initiated by three mechanisms: transformation from landslides, surface erosion and dam breaching. Due to rainfall infiltration, the hill slope gradually becomes saturated, and the soil loses its strength, causing shallow seated slope failures (Zhang et al., 2011). During a rainstorm, slope failures can occur at different times in space within a catchment. Some of the detached material may move into channels and form landslide dams, and some may transform into debris flows directly. As the surface runoff accumulates, the landslide dam formed earlier in the channel may break, initiating a channelized debris flow (e.g. Liu et al., 2009; Chen et al., 2012; Peng and Zhang, 2012). At the same time, the surface runoff may cause bed erosion and initiate hillslope debris flows (e.g. Cannon et al., 2001). Some of the separate debris flows may merge in the main channel of the drainage basin, forming a larger catastrophic debris flow event (e.g. Iverson et al., 1997). The final magnitude of a debris flow could be many times of its initial volume due to entrainment of materials along the path from additional slope failures, bed erosion or bank collapses (e.g. Iverson et al., 2011; Chen et al., 2012; Ouyang et al., 2015). If reaching a flat residential area downstream the basin, the developed debris flow can cause severe loss of lives and properties.

Based on the conceptual model for the whole process of debris flow in Fig. 2, the strategy of the integrated model, including two debris-flow initiation mechanisms (i.e. bed erosion and transformation from landslides) is shown in Fig. 3. The integrated model consists of a digital terrain module, a rainfall module, an infiltration module, an overland flow module, a slope stability module, a surface erosion module, a debris flow dynamics module

and a deposition module. The digital terrain module discretizes the study area into a grid system with geological, hydrological and geotechnical information for each cell assigned. All the computations are based on the concept of cell. As the primary triggering factor, rainfall is simulated in the rainfall module. Then water infiltration into the ground is simulated to analyze the pore water pressure profile and compute the surface runoff. The slope stability and surface erosion are then evaluated in the slope stability module and surface erosion module, respectively. Once debris flows are initiated by the two physical mechanisms, the motion of the flowing mixture is analyzed through the debris flow dynamics module. Material entrainment may occur along the flow path, incorporating solid materials from addition slope failures and surface erosion. Finally, the deposition process is assessed through the deposition module. The runout distance, inundation area and deposition volume of the debris flows can all be assessed.

2.2 Debris flow dynamics

The core of the proposed integrated analysis is the debris-flow dynamics simulation and constitutive modelling of the flowing mixture. The governing equations for debris flow dynamics describe the mixture movement and changes in debris flow properties, which are depth-integrated mass conservation equations (Equations 1 and 2) and momentum conservation equations (Equations 3) (Chen and Zhang, 2015):

$$\frac{\partial h}{\partial t}+\frac{\partial (hv)}{\partial x}=i[C_{v*}+(1-C_{v*})s_b]+A[C_{vA}+(1-C_{vA})s_A] \tag{1}$$

$$\frac{\partial (C_v h)}{\partial t}+\frac{\partial (C_v hv)}{\partial x}+=iC_{v*}+AC_{vA} \tag{2}$$

$$\frac{\partial v}{\partial t}+v\frac{\partial v}{\partial x}=g\left[-\mathrm{sgn}(v)S_f-\frac{\partial (z_b+h)}{\partial x}\right] - \frac{v\{i[C_{v*}+(1-C_{v*})s_b]+A[C_{vA}+(1-C_{vA})s_A]\}}{h} \tag{3}$$

where h is the flow depth; v is the depth-integrated flow velocity (m/s); i is the erosion rate (> 0) or deposition rate (< 0) (m/s); A is the rate of material entrainment from detached landslide materials (m/s); C_v is the volume fraction of solids in the flowing mixture; C_{v*} and C_{vA} are the volume fraction in the erodible bed and in the entrained materials, respectively; s_b and s_A are the degree of saturation of solids in the erodible bed and in the entrained materials, respectively; S_f is the energy slope; z_b is the bed elevation (m); and the sgn (i.e. signum) function is used to ensure that the direction of the flow resistance is opposite to that of the flow direction.

One of the requirements of the integrated analysis is modeling different flowing mixtures simultaneously. The flowing mixture can be classified into three types: clear water flow, hyperconcentrated flow, and fully developed debris flow based on sediment concentration, combining grain-size distribution and particle densities (Pierson, 2005). In this study, the flowing types of mixtures are classified using the volumetric solid concentration C_v, following FLO-2D Software Inc. (2009):

(1) If $C_v < 0.2$, the fluid mixture is deemed clear water flow which has a negligible yield stress and a dynamic viscosity like that of water;

(2) If $0.2 < C_v < 0.45$, a hyperconcentrated flow develops with a certain level of increased yield stress and dynamic viscosity;

(3) If $0.45 < C_v < 0.6$, the flowing mixture becomes a full debris flow with substantially increased yield stress and dynamic viscosity.

Therefore, a proper rheological model must involve C_v to account for the changing properties of the flowing mixture. We adopt different rheological models for different ranges of C_v to deal with this problem. For clear water flow of which C_v is less than 0.2, the energy slope S_f is based on Manning's equation. If $C_v > 0.2$, a quadratic rheological model developed by O'Brien et al. (1993) is used:

$$S_f = \frac{\tau_y}{\rho g h} + \frac{K\mu V}{8\rho g h^2} + \frac{n_{td}^2 V^2}{h^{4/3}} \quad (4)$$

where ρ is the mass density of the flowing mixture (kg/m^3); τ_y, μ and n_{td} are the yield stress (Pa), dynamic viscosity (Pa·s) and the equivalent Manning coefficient of the mixture, respectively; K is the laminar flow resistance. n_{td} is expressed as (FLO-2D Software Inc., 2009):

$$n_{td} = 0.0538ne^{6.0896C_v} \quad (5)$$

where n is the Manning coefficient. The following empirical relationships are adopted to estimate τ_y and μ (O'Brien and Julien, 1988):

$$\tau_y = \alpha_1 e^{\beta_1 C_v} \quad (6)$$

$$\mu = \alpha_2 e^{\beta_2 C_v} \quad (7)$$

where α_1, α_2, β_1, and β_2 are empirical coefficients.

2.3 Rainfall infiltration and convolution

Under heavy rainfall, the excess rainwater will become surface runoff when rainfall intensity exceeds the infiltration capacity. In EDDA 2.0, the infiltration capacity is assumed to be the saturated permeability of the surface soil. The surface runoff process is simulated by solving the governing equations (Eqs. 1-3) and Manning's equation with i, A and C_v equal to zero. The runoff water may cause surface erosion, or mix with landslide mass or flowing mixture, which will be described later.

Water infiltration will increase the subsurface pore water pressure, causing slope failures that are normally shallow-seated. The infiltration process is simulated in EDDA 2.0 by solving the Richards equation with a forward-time central-difference numerical solution. Non-uniform grid is created along the soil depth to enhance the accuracy of the solution near boundaries and interfaces. The integrated program calculates the instant pore water pressure

profile to facilitate evaluating the slope stability of each cell at each time step.

2.4 Initiation of debris flows from slope failures

A debris flow may be initiated by transformation from a mass flow of slope failure material at any location and at any time during a storm. The possible locations and approximate failing time can be identified in a cell-based slope stability analysis, if the topography, geology, soil properties etc. are defined properly. To consider this initiation mechanism, the slope instability evaluation must be performed over all the computational cells at each time step.

With the knowledge of real-time pore water pressure profiles provided by the infiltration module, a real-time slope instability analysis can follow. Considering that these rain-induced slope failures are shallow-seated, the thickness of the failure mass is small compared to the large plan dimensions of these slopes. Therefore, an infinite slope model for two-layer soil slopes is a reasonable option to evaluate the factor of safety (F_s) (Wu et al., 2016). Following Chen and Zhang (2014), the search for the minimum F_s goes from the ground surface to the wetting front where the volumetric water content changes significantly. If the minimum F_s is smaller than 1, slope failure will occur at the depth corresponding to the minimum F_s. The landslide mass is assumed to be a free-flowing mixture immediately after the slope failure, with a pre-defined C_v value for the soil deposit and a flow depth the same as the failure depth.

2.5 Initiation of debris flows due to bed erosion

Intense rainfall can generate plentiful surface runoff, and the soil bed will erode in the runoff water. The initially clear overland flow can gradually develop into a hyperconcentrated flow and finally into a hillslope debris flow, as its C_v value increases through entrainment from bed erosion. To consider this initiation mechanism, the erosion process is analyzed

within each computational cell at each time step.

We consider the occurrence of erosion under the condition that the bed shear stress is equal or larger than the critical erosive shear stress of the bed material and the volumetric sediment concentration is smaller than an equilibrium value. The equilibrium value proposed by Takahashi et al. (1992) is adopted in this study:

$$C_{v\infty} = \frac{\rho_w \tan\theta}{(\rho_s - \rho_w)(\tan\phi_{bed} - \tan\theta)} \tag{8}$$

where ϕ_{bed} is the internal friction angle of the erodible bed; ρ_s is the density of soil particles (kg/m^3); ρ_w is the density of water (kg/m^3); and θ is the slope angle.

Many researchers have studied the relationship between the soil erosion rate and shear stress. A form of exponential expression has been used for bed erosion in the literature (e.g. Roberts et al., 1998; Chen et al., 2015). More widely used is a linear function of shear stress (e.g. Graf, 1984; Hanson and Simon, 2001; Julian and Torres, 2006; Chang et al., 2011; Chen and Zhang, 2015):

$$i = K_e(\tau - \tau_c) \tag{9}$$

where i is the erosion rate (m/s); τ is the shear stress at the soil-water interface (Pa); K_e is the coefficient of erodibility (m^3/N-s); τ_c is the critical erosive shear stress at the initiation of bed erosion (Pa). The latter two parameters describe the erosion resistance of the bed soil and are related to soil index properties (e.g. Chang et al., 2011; Zhu and Zhang, 2016). The shear stress acting on the bed can be expressed as (e.g. Graf, 1984):

$$\tau = \rho g h S_f \tag{10}$$

where S_f is the energy slope.

2.6 Material exchange: entrainment and deposition

Material exchange occurs as debris flow marches along its flowing path, including

material entrainment (solid mass gain from outside of the flowing mixture) and deposition (solid mass loss from inside of the flowing mixture).

The entrainment from additional bed erosion or slope failure materials along its trajectory plays a significant role in debris flow volume amplification. The final volume of the debris flow deposit could be many folds of its initial volume. An excellent example is the 1990 Tsing Shan debris flow that was the largest ever observed in Hong Kong. An originally small slip of 350 m^3 developed into a final volume of 20,000 m^3 by entraining colluvium along its flow path (King, 1996). In the integrated model, the landslide mass and surface erosion are considered as the sources of material entrainment. The slope stability and surface erosion evaluation module will be called for every computational cell at every time step; hence the entrainment process is automatically considered once the two modules are called.

After flowing into a flatter area, deposition of some solid material will occur. Deposition is deemed to occur if the flow velocity is smaller than a critical value and C_v is larger than the equilibrium value described in Eq. 8. The deposition rate can be expressed as

$$i = \delta_d \left(1 - \frac{V}{pV_e}\right) \frac{C_{v\infty} - C_v}{C_{v*}} V \tag{11}$$

where V_e is the critical flow velocity following Takahashi et al. (1992); δ_d is a coefficient of deposition rate; p (< 1) is a coefficient accounting for the location difference, and a value of 0.67 is recommended (Takahashi et al., 1992); V is the flow velocity; C_{v*} is the volume fraction of solids in the erodible bed. The deposition condition is also detailed in Chen and Zhang (2015).

2.7 Numerical scheme

The terrain is discretized into a grid of cells. Each cell is assigned with the input data, including topography, soil depth, geotechnical soil properties, rheological model parameters

276 etc. There are eight flow directions in each cell: four compass directions and four diagonal
277 directions. In each time step, the infiltration is evaluated first to compute the surface runoff
278 and slope stability at each cell. Then changes in flow depth h and volumetric sediment
279 concentration C_v within each cell are evaluated considering the surface runoff, slope failure
280 mass entrainment, erosion, and deposition, followed by computing the flow velocity,
281 discharge and density along the eight flow directions of all the cells, with the averaged
282 surface roughness and slope between two cells computed. The changes in h and C_v due to the
283 flow exchange are evaluated finally at each cell.

284 After all the computations have been completed in each time step, numerical stability
285 criteria are checked for each cell to limit the time step to avoid surging while allowing for
286 large time steps. Three convergence criteria are adopted:

287 (1) The Courant-Friedrichs-Lewy (CFL) condition, with the physical interpretation that a
288 particle of fluid should not travel more than the cell size in one time step (Fletcher,
289 1990), is mostly used in explicit schemes. The time step is limited by

290 $$\Delta t \le C\Delta x / (\beta V + c) \quad (12)$$

291 where C is the Courant number (C is not smaller than or equal to 1); m is a coefficient
292 (5/3 for a wide channel); c is the computed wave celerity.

293 (2) The percent change of flow depth in one time step should not exceed a specified
294 tolerant value, TOLP(h);

295 (3) The change in flow depth in one time step should not exceed a specified tolerant
296 value, TOL(h), which is applied when the flow moves to a cell with zero flow depth.

297 Adjusting these three criteria, the computational time and accuracy could reach a good
298 balance. If all the numerical stability criteria are successfully satisfied, the time step can be
299 increased for the next computational cycle. Otherwise the time step will be reduced and the
300 computation restarted. The volume conservation is computed at the end of each time step for

301 the inflow, outflow, grid system storage and infiltration loss.

302

303 **3 Model verification**

304 The previous version, EDDA 1.0 (Chen and Zhang, 2015), has passed several
305 verification tests including debris flow dynamics, erosion and deposition. In this new version
306 of integrated analysis, the new modules for surface runoff, coupled infiltration and slope
307 stability analysis, and the integrated program require further verification. The response of
308 Xiaojiagou Ravine during a rainstorm in August 2010 is used to verify the new modules. The
309 in-situ conditions shortly after the 2010 Xiaojiagou debris flow event are shown in Fig. 4.
310 The Xiaojiagou Ravine has an area of 7.84 km^2. The elevation of the ravine ranges between
311 1,100 m and 3,200 m. The hill slopes within the ravine are very steep with an average slope
312 angle of 46°. There are one main drainage channel and four branches within the Xiaojiagou
313 Ravine. The loose soil deposits on the hill slopes and channels of the ravine before the debris
314 flow event are identified based on field investigations and interpretation of satellite image
315 (e.g. Chen and Zhang, 2014). The rainstorm process triggering the catastrophic Xiaojiagou
316 debris flow is presented in Fig. 5. The rainstorm lasted about 40 hours with a total
317 precipitation of 220 mm.

318 First the performance of the rainfall-runoff module of the integrated program is
319 compared with a commonly used program FLO-2D (FLO-2D Software Inc., 2009). Then, the
320 infiltration module is checked against an analytical solution under steady rainfall. The slope
321 stability analysis is verified by comparing with the landslide satellite image and the
322 computation results by Chen and Zhang (2014). Finally, the performance of the integrated
323 model is checked against the 2010 Xiaojiagou debris flow event in Section 4.

324

325

3.1 Verification test 1: rainfall runoff

The same input data are used in EDDA 2.0 and FLO-2D, including the digital elevation model, Manning's coefficient (n = 0.3), the limiting Froude number (L_f = 0.8), the saturated permeability of the surface soil (k_{st} = 3.6 mm/h or 10^{-6} m/s) and the rainfall data (Fig. 5). Other hydrological parameters such as the soil porosities used in FlO-2D are adopted following Chen et al. (2013) and Shen et al. (2017).

The results from the two programs are compared in Fig. 6, including the distributions of the maximum flow depth and flow velocity. The result from FlO-2D (Figs. 6a and 6c) differ only slightly from those of EDDA 2.0 (Figs. 6b and 6d). During the rainstorm process, the maximum flow depth computed by FLO-2D is 3.2 m, while that by EDDA 2.0 is 3.4 m. The outflow hydrographs recorded at the mouth of the ravine of the two programs are shown in Fig. 7. The computed overall discharge processes from both programs are very close.

3.2 Verification test 2: infiltration process and resulting pore-water pressure changes

Before applying the infiltration module to compute the pore water pressure profiles under the actual rainfall event, four cases of infiltration under steady rainfall are adopted to verify the infiltration module. The results are compared with those from an analytical solution by Srivastava and Yeh (1991) and Zhan et al. (2013). The scenario of two-layer soil is considered, which is also used in the field application. Table 1 presents the input parameters for the four cases. Four combinations are set up to represent likely in-situ conditions. The results from the numerical infiltration module and the analytical solution are compared in Fig. 8. For all the four cases, the module performance is satisfactory.

3.3 Verification test 3: slope stability analysis

The 2008 Wenchuan earthquake triggered over 50,000 landslides within the earthquake

region, leaving a large amount of loose materials on hill slopes and in channels (Fig. 4). These materials became the source of numerous post-earthquake rain-induced landslides and debris flows. Until now, nearly 80% of such materials remained in the mountain regions, posing great potential threats (Zhang et al., 2016). EDDA 2.0 is used to reproduce the slope failures under the rainstorm in August 2010 (Fig. 5) by Chen and Zhang (2014), who evaluated the slope stability of a 164.5 km^2 area near the epicenter. All the parameters are the same as those in that study, with the only difference being that the area concerned in this study is only Xiaojiagou Ravine (Fig. 4). The loose soil deposits are assumed to be two layers. Given the same parameters such as the topography, layer thicknesses and soil properties, the unstable cells when rainfall terminates are computed using the slope failure module. Comparing the simulation results with the observation (Fig. 9), the computed unstable cells generally fall upon the landslide scars formed during the rainstorm event. Moreover, the results are compared with those by Chen and Zhang (2014), which have been verified using the confusing matrix method (e.g. Van Den Eeckhaut et al., 2006). It is found that the results of the two separate analyses are very similar. The computed total scar area is 4.42×10^5 m^2, comparing well with 5.20×10^5 m^2 from the satellite image. The difference is 15%. It is concluded that the proposed slope stability module performs reasonably well.

4 Field application

4.1 Xiaojiagou debris flow on 14 August 2010

A heavy rainstorm swept the epicenter, Yinxiu town, and its vicinity. The rainstorm lasted about 40 h from 12 to 14 August 2010, pouring about 220 mm of precipitation in total (Fig. 5). A catastrophic debris flow was triggered by the storm in Xiaojiagou Ravine (Fig. 4). The debris flow was witnessed at the ravine mouth at about 5:00 am on 14 August and lasted about 30 min. About 1.17×10^6 m^3 of the soil deposit was brought out of the Xiaojiagou

Ravine mouth in a form of a channelized debris flow. The runout material deposited in front of the mouth, burying 1100 m of Province Road 303 (PR303), blocking Yuzixi River, forming a debris flow barrier and raising the river bed by at least 15 m.

4.2 Input information

In EDDA 1.0, the study area has to be divided into two domains for rainfall runoff simulation and debris-flow runout simulation respectively. However, in the integrated simulation by EDDA 2.0, only one grid of 9500 cells 30 × 30 m in size is created (Fig. 2). After the Xiaojiagou debris flow, detailed field investigations and laboratory tests were conducted (Chen et al., 2012), as well as numerical back analysis (Chen et al., 2013). The study area is divided into four zones by satellite interpretation: bare soil, vegetated soil, bed rock and river bed (Chen and Zhang, 2014). The soil properties of each zone and the constitutive (or rheological) parameters used in the integrated simulation are determined following EDDA 1.0 (Chen and Zhang, 2015), shown in Tables 2-4. The erosion resistance parameters τ_c and K_e of the soils are determined using the empirical equations based on field tests in the Wenchuan earthquake zone (Chang et al., 2011):

$$\tau_c = 6.8 PI^{1.68} P^{-1.73} e^{-0.97} \tag{13}$$

$$K_e = 0.020075 e^{4.77} C_u^{-0.76} \tag{14}$$

where e is the void ratio; PI is the plasticity index; P is the fines content (< 0.063 mm); C_u is the coefficient of uniformity. These four soil properties are determined to be 1.05, 18, 14 and 2000, respectively, according to Chang et al. (2011). Therefore, τ_c and K_e are estimated to be 8.7 Pa and 7.8×10^{-8} m^3/N-s, respectively.

4.3 Integrated simulation results

We examine the final output of the integrated simulation first. Erosion plays an

important role in the volume magnification of debris flows. The final erosion depths in the eroded areas are shown in Fig. 10a. The most eroded areas during the Xiaojiagou debris flow event were in channels, where a huge amount of loose solid material was present (Chen et al., 2012). Loose deposits on the hill slopes also eroded after the landslide bodies detached from their original locations and slid down the slopes. The distribution of the eroded areas reflects that the debris flows were initiated from both slope failures and surface erosion, then developed along the channels by further erosion and entrainment of the slope failure materials, which are the two mechanisms considered in the integrated model. The distribution of the maximum flow velocity is shown in Fig. 10b, with the maximum value being 9.5 m/s, which is very close to that from EDDA 1.0 (9.1 m/s). The slightly larger value of flow velocity from EDDA 2.0 is attributed to the consideration of the extra surface runoff within domain two created when using EDDA 1.0 (Fig. 2). The maximum velocity occurs in the ravine channels, indicating that the debris flow moves very rapidly.

The simulated and observed deposition areas are compared in Fig. 11. It is seen that the simulation results (Fig. 11a) match the observation (Fig. 11b) reasonably well. The simulated deposition depth is approximately 20 m, very close to that of the observed thickness of the deposit fan during the field investigations. The total volume of the observed deposition fan is about 1.17×10^6 m^3, while the simulated deposition volume of the debris flow is 0.9×10^6 m^3. The integrated model evaluates a smaller debris flow volume and the difference is about 23%. The main uncertainty arises from the slope failure module and surface erosion module.

The changes in the volumetric sediment concentration C_v and the discharge hydrograph at Section 1-1 (Fig. 4) are recorded during the simulation of the whole rainfall process, shown in Fig. 12. The integrated model simulates two peaks in the discharge process throughout the rainfall with a precursory boulder front arriving in advance. At around 12 h, the value of C_v increases very quickly to a peak value of 0.6, indicating the arrival of the debris flow.

Afterwards, C_v decreases, which can be viewed as a hyperconcentrated flow or a clear water flow after the debris flow passes. Another large debris flow surge is simulated at around 32 h with the same pattern as the first one. The debris flow passes through Section 1-1 (Fig. 4) first and continues to develop for some time. After most of the solid materials are brought away by the debris flow surge, the flow at Section 1-1 becomes a hyperconcentrated flow, and the flowing mixture gradually becomes a clear water flow as the rainwater continues to generate surface runoff without further material entrainment. The integrated simulation is capable of simulating multiple debris flow surges and the changes in the flowing mixture properties throughout a rainfall event.

To demonstrate the evolution of the flowing mixture within the drainage basin, the distributions of C_v at four snapshots during the storm are shown in Fig. 13. The recording times of these four figures span a complete evolution cycle, i.e. clear water flow (Fig. 13a), debris flow initiation (Fig. 13b), debris flow motion (Fig. 13c), and hyperconcentrated flow/clear water flow (Fig. 13d). This evolution cycle could occur within the basin several times in different branch channels, which can be captured by the integrated model.

5 Limitations of EDDA 2.0

We have successfully extended the “two-step” debris-flow simulation to an integrated simulation of the whole process of rain-induced debris flows. However, there are still limitations in the underlying assumptions and simplifications:

1. EDDA 2.0 considers the initiation of debris flows from transformation of slope failures and surface erosion. However, the initiation from dam breaching has not yet been tested.
2. The studies consider material entrainment from surface erosion and slope failure detachment, but the entrainment from bank failures can only be considered using an

empirical rate, instead of through a three-dimensional physical model.

3. The governing equations are in a depth-integrated form; hence particle segregation in the vertical direction cannot be considered.
4. The rheological models for the hyperconcentrated flow, fully developed debris flow and slope failure mass flow need further study. Particularly, the slope failure mass movement is critical for estimating the transformation rate from a slope failure to a debris flow.

6 Summary and conclusions

A new integrated simulation model is developed for simulating rain-induced debris-flow initiation, motion, entrainment, deposition and property changes. The model is unique in that it simulates the whole process of rain-induced debris flow evolution and two physical initiation mechanisms (i.e. transformation from landslides and surface erosion). Previous "two-step analysis" with an assumed inflow hydrograph and an inflow location can now be conducted at one go scientifically without subjective assumptions.

Three numerical tests have been conducted to verify the performance of the newly added modules of the integrated model. The Xiaojiagou Ravine landslides and debris flows triggered by the rainstorm in August 2010 were used as a verification case. In test 1, the rainfall runoff simulation by EDDA 2.0 was compared to FLO-2D. The simulation results from the two models are very close, which indicates that EDDA 2.0 simulates rainfall runoff well. In test 2, an analytical solution for evaluating pore water pressure profile under infiltration is adopted. Comparison between the model solution and the analytical solution indicates that the integrated model evaluates the infiltration process well. The regional slope stability within the study area under the same rainstorm was evaluated using the integrated model in test 3. The computed unstable cells compare well with the observations from

satellite images and the results from previous studies.

The new integrated model was finally applied to reproduce the Xiaojiagou debris flow event. The model can simulate the entire evolution process of rain-induced debris flows, and estimates reasonably well the volume, inundated area and runout distance of the debris flow. It is concluded that the new integrated debris flow simulation model, EDDA 2.0, is capable of (1) simulating the whole process of rain-induced debris flow from debris-flow initiation to post-initiation debris-flow motion, entrainment and deposition, and (2) tracing the evolution of the flowing mixture in time and space during the whole process of rainfall. The integrated model will serve as a powerful tool for analyzing multi-hazard processes and hazard interactions, and assessment of regional debris-flow risks in the future.

Code availability. EDDA 2.0 is written in FORTRAN, which can be compiled using Intel FORTRAN Compilers. A doi has been generated for the source code and the source code is available online at http://doi.org/10.5281/zenodo.1033377. The source code is also available online as a supplementary material to this paper. The main subroutine is “dfs.F90”, which presents the numerical solution algorithm for evaluating debris flow initiation from erosion and slope failures, and for solving the governing equations of the dynamics of the flowing mixture. An input file is needed (“edda_in.txt”) for inputting material properties, hydrological and rheological parameters and control settings. As an integrated program, EDDA 2.0 can be used to analyse regional slope failures, so the “edda_in.txt” file also includes the material properties and controlling options for slope stability analysis. Another input file (“outflow.txt”) is required to define the outflow cell. Digital terrain data (e.g. surface elevation, slope gradient and erodible layer thickness) are included in separate ASCII grid files and enclosed in the data folder. Output files are stored in the results folder and output variables at selected points are stored in “EDDALog.txt”.

Author contributions. Limin Zhang and Ping Shen conceived the methodology and formulated the model. Ping Shen programmed the analysis code and performed the analysis. Hongxin Chen and Ruilin Fan evaluated the model results. All authors contributed to the writing of the manuscript.

Competing interests. The authors declare that they have no conflict of interest.

Acknowledgements. The authors acknowledge the support from the Research Grants Council of the Hong Kong SAR (No. C6012-15G and No. 16206217).

References

Archfield, S. A., Steeves, P. A., Guthrie, J. D., and Ries III, K. G.: Towards a publicly available, map-based regional software tool to estimate unregulated daily streamflow at ungauged rivers, Geosci. Model Dev., 6, 101-115, doi:10.5194/gmd-6-101-2013, 2013.

Baum, R. L. and Godt, J. W.: Early warning of rainfall-induced shallow landslides and debris flows in the USA, Landslides, 7(3), 259-272, doi: 10.1007/s10346-009-0177-0, 2010.

Bartelt, P., Buehler, Y., Christen, M., Deubelbeiss, Y., Graf, C., McArdell, B., Salz, M., and Schneider, M.: A numerical model for debris flow in research and practice, User Manual v1.5 Debris Flow, WSL Institute for Snow and Avalanche Research SLF, Switzerland, 2013.

Beguería, S., Van Asch, Th. W. J., Malet, J.-P., and Gröndahl, S.: A GIS-based numerical model for simulating the kinematics of mud and debris flows over complex terrain, Nat. Hazard Earth Sys., 9, 1897-1909, doi:10.5194/nhess-9-1897-2009, 2009.

Berti, M. and Simoni, A.: Experimental evidences and numerical modelling of debris flow

initiated by channel runoff, Landslides, 2, 171-182, doi:10.1007/s10346-005-0062-4, 2005.

Berti, M., Martina, M. L. V., Franceschini, S., Pignone, S., Simoni, A., and Pizziolo, M.: Probabilistic rainfall thresholds for landslide occurrence using a Bayesian approach, J. Geophys. Res-Earth, 117(4), doi:10.1029/2012JF002367, 2012.

Boetticher, A. V., Turowski, J. M., McArdell, B. W., Rickenmann, D., and Kirchner, J. W.: DebrisInterMixing-2.3: a finite volume solver for three-dimensional debris-flow simulations with two calibration parameters - Part 1: Model description, Geosci. Model Dev., 9, 2909-2923, doi:10.5194/gmd-9-2909-2016, 2016.

Boss Corporation: DAMBRK-User's manual, Boss International Inc., Madison, Wisconsin, USA, 1989.

Caine, N.: The rainfall intensity: duration control of shallow landslides and debris flows, Geogr. Ann. A, 62, 23-27, doi: 10.2307/520449, 1980.

Cannon, S. H., Kirkham, R. M., and Parise, M.: Wildfire-related debris-flow initiation processes, Storm King Mountain, Colorado, Geomorphology, 39, 171-188, doi:10.1016/S0169-555X(00)00108-2, 2001.

Cannon, S. H., Gartner, J. E., Wilson, R., Bowers, J., and Laber, J.: Storm rainfall conditions for floods and debris flows from recently burned areas in southwestern Colorado and southern California, Geomorphology, 96(3-4), 250-269, doi: 10.1016/j.geomorph.2007.03.019, 2008.

Chang, D. S., Zhang, L. M., Xu, Y., and Huang, R. Q.: Field testing of erodibility of two landslide dams triggered by the 12 May Wenchuan earthquake, Landslides, 8, 321-332, doi:10.1007/s10346-011-0256-x, 2011.

Chen, C. Y., Chen, T. C., Yu, F. C., Yu, W. H., and Tseng, C. C.: Rainfall duration and debris-flow initiated studies for real-time monitoring, Environ. Geol., 47, 715-724,

551 doi:10.1007/s00254-004-1203-0, 2005.
552 Chen, H. X. and Zhang, L. M.: A physically-based distributed cell model for predicting
553 regional rainfall-induced shallow slope failures, Eng. Geol., 176, 79-92,
554 doi:10.1016/j.enggeo.2014.04.011, 2014.
555 Chen, H. X. and Zhang, L. M.: EDDA 1.0: integrated simulation of debris flow erosion,
556 deposition and property changes, Geosci. Model Dev., 8, 829-844,
557 doi:10.5194/gmd-8-829-2015, 2015.
558 Chen, H. X., Zhang, L. M., Chang, D. S., and Zhang, S.: Mechanisms and runout
559 characteristics of the rainfall-triggered debris flow in Xiaojiagou in Sichuan Province,
560 China, Nat. Hazards, 62, 1037-1057, doi:10.1007/s11069-012-0133-5, 2012.
561 Chen, H. X., Zhang, L. M., Zhang, S., Xiang, B., and Wang, X. F.: Hybrid simulation of the
562 initiation and runout characteristics of a catastrophic debris flow, J. Mt. Sci., 10,
563 219-232, doi:10.1007/s11629-013-2505-z, 2013.
564 Chen, N. S., Zhou, W., Yang, C. L., Hu, G. S., Gao, Y. C., and Han, D.: The processes and
565 mechanism of failure and debris flow initiation for gravel soil with different clay
566 content, Geomorphology, 121, 222-230, doi:10.1016/j.geomorph.2010.04.017, 2010.
567 Chen, Z., Ma, L., Yu, S., Chen, S., Zhou, X., Sun, P., and Li, X.: Back analysis of the draining
568 process of the Tangjiashan barrier lake, J. Hydraul Eng., 141(4), 05014011, doi:
569 10.1061/(ASCE)HY.1943-7900.0000965, 2015.
570 Coe, J. A., Kinner, D. A., and Godt, J. W.: Initiation conditions for debris flows generated by
571 runoff at Chalk Cliffs, central Colorado, Geomorphology, 96, 270-297,
572 doi:10.1016/j.geomorph.2007.03.017, 2008.
573 Cui, P.: Study on condition and mechanisms of debris flow initiation by means of experiment,
574 Chinese Sci. Bull., 37, 759-763, 1992.
575 De Luca D. L. and Versace P. A.: Comprehensive framework for empirical modeling of

landslides induced by rainfall: the Generalized FLaIR Model (GFM), Landslides, 14(3), 1009-1030, ISSN: 1612-5118, DOI: 10.1007/s10346-016-0768-5, 2017a.

De Luca, D. L. and Versace, P.: Diversity of Rainfall Thresholds for early warning of hydro-geological disasters, Adv. Geosci., 44, 53-60, https://doi.org/10.5194/adgeo-44-53-2017, 2017b.

Fletcher, C. A. J.: Computational Techniques for Fluid Dynamics, Volume I, 2nd ed., Springer-Velag, New York, 1990.

FLO-2D Software Inc.: FLO-2D reference manual, Nutrioso, Arizona, USA, 2009.

Formetta, G., Mantilla, R., Franceschi, S., Antonello, A., and Rigon, R.: The JGrass-NewAge system for forecasting and managing the hydrological budgets at the basin scale: models of flow generation and propagation/routing, Geosci. Model Dev., 4, 943-955, doi:10.5194/gmd-4-943-2011, 2011.

Gao, L., Zhang, L. M., Chen, H. X., and Shen, P.: Simulating debris flow mobility in urban settings, Eng. Geol., 214, 67-78, doi:10.1016/j.enggeo.2016.10.001, 2016.

Gao, L., Zhang, L. M., and Cheung, R. W. M.: Relationships between natural terrain landslide magnitudes and triggering rainfall based on a large landslide inventory in Hong Kong, Landslides, DOI: 10.1007/s10346-017-0904-x, 2017.

Godt, J. W., Baum, R. L., and Chleborad, A. F.: Rainfall characteristics for shallow landsliding in Seattle, Washington, USA. Earth Surf. Proc. Land, 31, 97-110, doi: 10.1002/esp.1237, 2006.

Graf, W. H.: Hydraulics of sediment transport, Water Resources Publications, Colorado, 1984.

Guzzetti, F., Peruccacci, S., Rossi, M., and Stark, C. P.: The rainfall intensity-duration control of shallow landslides and debris flows: An update, Landslides, 5, 3-17, doi: 10.1007/s10346-007-0112-1, 2008.

Hanson, G. J. and Simon, A.: Erodibility of cohesive streambeds in the loess area of the midwestern USA, Hydrolo. Process., 15(1), 23-38, doi: 10.1002/hyp.149, 2001.

Hungr, O.: A model for the runout analysis of rapid flow slides, debris flows, and avalanches, Can. Geotech. J., 32, 610-623, doi:10.1139/t95-063, 1995.

Hungr, O. and McDougall, S.: Two numerical models for landslide dynamic analysis, Computat. Geosci., 35(5), 978-992, doi: 10.1016/j.cageo.2007.12.003, 2009.

Iverson, R. M.: The physics of debris flows, Rev. Geophys., 35(3), 245-296, doi: 10.1029/97RG00426, 1997.

Iverson, R. M., Reid, M. E., and LaHusen, R. G.: Debris-flow mobilization from landslides, Annu. Rev. Earth Pl. Sc., 25(1), 85-138, doi: 10.1146/annurev.earth.25.1.85, 1997.

Iverson, R. M., Reid, M. E., Logan, M., LaHusen, R. G., Godt, J. W., and Griswold, J. P.: Positive feedback and momentum growth during debris-flow entrainment of wet bed sediment, Nat. Geosci., 4, 116-121, doi:10.1038/ngeo1040, 2011.

Johnson, K. A. and Sitar, N.: Hydrologic conditions leading to debris-flow initiation, Can. Geotech. J., 27, 789-801, doi:10.1139/t90-092, 1990.

Julian, J. P. and Torres, R.: Hydraulic erosion of cohesive riverbanks, Geomorphology, 76(1-2), 193-206, doi: 10.1016/j.geomorph.2005.11.003, 2006.

Kappes, M. S., Keiler, M., von Elverfeldt, K. and Glade, T.: Challenges of analyzing multi-hazard risk: a review, Nat. Hazards, 64(2), 1925-1958, doi: 10.1007/s11069-012-0294-2, 2012.

King, J.: Tsing Shan debris flow, Special Project Report SPR 6/96, Geotechnical Engineering Office, Hong Kong Government, 133, 1996.

Kwan, J. S. and Sun, H.: An improved landslide mobility model, Can. Geotech. J., 43(5), 531-539, doi: 10.1139/t06-010, 2006.

Lee, B. Y., Mok, H. Y., and Lee, T. C.: The latest on climate change in Hong Kong and its

implications for the engineering sector, DHKO in the HKIE Conf. on Climate Change - Hong Kong Engineers' Perspective, Hong Kong Observatory, Government of Hong Kong SAR, Hong Kong, 2010.

Liu, K. F. and Huang, M. C.: Numerical simulation of debris flow with application on hazard area mapping, Computat. Geosci., 10, 221-240, doi: 10.1007/s10596-005-9020-4, 2006.

Liu, N., Zhang, J. X., Lin, W., Cheng, W. Y., and Chen, Z. Y.: Draining Tangjiashan Barrier Lake after Wenchuan Earthquake and the flood propagation after the dam break, Sci. China Ser. E., 52(4), 801–809, doi: 10.1007/s11431-009-0118-0, 2009.

Marzocchi, W., Garcia-Aristizabal, A., Gasparini, P., Mastellone, M. L., and Di Ruocco, A.: Basic principles of multi-risk assessment: a case study in Italy, Nat. Hazards, 62(2), 551-573, doi: 10.1007/s11069-012-0092-x, 2012.

Medina, V., Hürlimann, M., and Bateman, A.: Application of FLATModel, a 2-D finite volume code, to debris flows in the northeastern part of the Iberian Peninsula, Landslides, 5, 127-142, doi: 10.1007/s10346-007-0102-3, 2008.

O'Brien, J. S. and Julien, P. Y.: Laboratory analysis of mudflow properties, J. Hydraul. Eng., 114, 877-887, doi: 10.1061/(ASCE)0733-9429(1988)114:8(877), 1988.

O'Brien, J. S., Julien, P. Y., Fullerton, W. T.: Two-dimensional water flood and mudflow simulation, J. Hydraul. Eng., 119, 244-261, doi: 10.1061/(ASCE)0733-9429(1993)119:2(244), 1993.

Ouyang, C., He, S., and Tang, C.: Numerical analysis of dynamics of debris flow over erodible beds in Wenchuan earthquake-induced area, Eng. Geol., 194, 62-72, doi: 10.1016/j.enggeo.2014.07.012, 2015.

Pastor, M., Haddad, B., Sorbino, G., Cuomo, S., and Drempetic, V.: A depth-integrated, coupled SPH model for flow-like landslides and related phenomena, Int. J. Numer. Anal. Met., 33(2), 143-172, doi: 10.1002/nag.705, 2009.

Peng, M., and Zhang, L.M.: Breaching parameters of landslide dams, Landslides, 9(1): 13–31, doi: 10.1007/s10346-011-0271-y, 2012.

Pierson, T. C.: Hyperconcentrated flow - transitional process between water flow and debris flow. In Debris-flow hazards and related phenomena (eds. Jakob, M. and Hungr, O.), Springer-Praxis, Chichester, UK, 159-202, doi: 10.1007/3-540-27129-5_8, 2005.

Quan Luna, B., Blahut, J., van Asch, T., van Westen, C., and Kappes, M.: ASCHFLOW-A dynamic landslide run-out model for medium scale hazard analysis, Geoenvironmental Disasters, 3(1), 29, 10.1186/s40677-016-0064-7, 2016.

Raia, S., Alvioli, M., Rossi, M., Baum, R. L., Godt, J. W., and Guzzetti, F.: Improving predictive power of physically based rainfall-induced shallow landslide models: a probabilistic approach, Geosci. Model Dev., 7, 495-514, doi:10.5194/gmd-7-495-2014, 2014.

Roberts, J., Jepsen, R., Gotthard, D., and Lick, W.: Effects of particle size and bulk density on erosion of quartz particles, J. Hydraul Eng., doi: 10.1061/(ASCE)0733-9429(1998)124:12(1261), 1261-1267, 1998.

Shen, P., Zhang, L. M., Chen, H. X., and Gao, L.: Role of vegetation restoration in mitigating hillslope erosion and debris flows, Eng. Geol., 216, 122-133, doi: 10.1016/j.enggeo.2016.11.019, 2017.

Srivastava, R. and Yeh, T. C. J.: Analytical solutions for one-dimensional, transient infiltration toward the water table in homogeneous and layered soils, Water Resour. Res., 27, 753-762, doi:10.1029/90WR02772, 1991.

Staley, D. M., Kean, J. W., Cannon, S. H., Schmidt, K. M., and Laber, J. L.: Objective definition of rainfall intensity–duration thresholds for the initiation of post-fire debris flows in southern California, Landslides, 10(5), 547-562, doi: 10.1007/s10346-012-0341-9, 2013.

676 Takahashi, T.: Debris flow, Annu. Rev. Fluid Mech., 13, 57-77, 1981.
677 Takahashi, T.: Debris flow: mechanics, prediction and countermeasures, Taylor & Francis,
678 London, UK, 2007.
679 Takahashi, T., Nakagawa, H., Harada, T., and Yamashiki, Y.: Routing debris flows with
680 particle segregation, J. Hydraul. Eng., 118, 1490-1507,
681 doi:10.1061/(ASCE)0733-9429(1992)118:11(1490), 1992.
682 Tang, C., Rengers, N., van Asch, Th.W.J., Yang, Y. H., and Wang, G. F.: Triggering conditions
683 and depositional characteristics of a disastrous debris flow event in Zhouqu city, Gansu
684 Province, northwestern China, Nat. Hazard Earth Sys., 11, 2903-2912,
685 doi:10.5194/nhess-11-2903-2011, 2011.
686 Van Den Eeckhaut, M., Vanwalleghem, T., Poesen, J., Govers, G., Verstraeten, G.,
687 Vandekerckhove, L.: Prediction of landslide susceptibility using rare events logistic
688 regression: a case-study in the Flemish Ardennes (Belgium), Geomorphology, 76(3),
689 392-410, doi: 10.1016/j.geomorph.2005.12.003, 2006.
690 Wieczorek, G. F.: Effect of rainfall intensity and duration on debris flows in central Santa
691 Cruz Mountains, California, Rev. Eng. Geol., 7, 93-104, doi:10.1130/REG7-p93, 1987.
692 Wong, H. N.: Rising to the challenges of natural terrain landslides, Natural Hillsides: Study
693 and Risk Management Measures, Proc., 29th Annual Seminar of the HKIE Geotechnical
694 Division, Hong Kong Institution of Engineers, Hong Kong, 15-53, 2009.
695 Wu, L. Z., Selvadurai, A. P. S., Zhang, L. M., Huang, R. Q., and Huang, J.: Poro-mechanical
696 coupling influences on potential for rainfall-induced shallow landslides in unsaturated
697 soils, Adv. Water Resour., 98, 114-121, doi: 10.1016/j.advwatres.2016.10.020, 2016.
698 Zhan, T. L., Jia, G. W., Chen, Y. M., Fredlund, D. G., and Li, H.: An analytical solution for
699 rainfall infiltration into an unsaturated infinite slope and its application to slope stability
700 analysis, Int. J. Numer. Anal. Met., 37, 1737-1760, doi:10.1002/nag.2106, 2013.

Zhang, L. L., Zhang, J., Zhang, L. M., and Tang, W. H.: Stability analysis of rainfall-induced slope failure: a review, Proceedings of the ICE-Geotechnical Engineering, 164, 299, 2011.

Zhang, L. M., Zhang, S., and Huang, R. Q.: Multi-hazard scenarios and consequences in Beichuan, China: The first five years after the 2008 Wenchuan earthquake, Engineering Geology, 180, 4-20, 2014.

Zhang, S., Zhang, L. M., Chen, H. X., Yuan, Q., and Pan, H.: Changes in runout distances of debris flows over time in the Wenchuan Earthquake zone, J. Mt. Sci., 10, 281-292, doi:10.1007/s11629-012-2506-y, 2013.

Zhang, S., Zhang, L. M., Lacasse, S., and Nadim, F.: Evolution of mass movements near epicentre of Wenchuan earthquake, the first eight years. Sci. Rep., 6, 36154, 2016.

Zhou, W. and Tang, C.: Rainfall thresholds for debris flow initiation in the Wenchuan earthquake-stricken area, southwestern China, Landslides, 11, 877-887, doi:10.1007/s10346-013-0421-5, 2014.

Zhu, H., and Zhang, L.M.: Field investigation of erosion resistance of common grass species for soil-bioengineering in Hong Kong, Acta Geotechnica, 11(5), 1047–1059, doi: 10.1007/s11440-015-0408-6, 2016.

718 **List of Captions**

719

720 ***Table captions***

721 **Table 1.** Parameters used in the infiltration module verification.

722 **Table 2.** Properties of four types of superficial materials.

723 **Table 3.** Soil properties for debris flow simulation.

724 **Table 4.** Constitutive (rheological) parameters for debris flow simulation.

725

726 ***Figure captions***

727 **Figure 1.** Conceptual model of a rain-induced debris flow and three typical initiation
728 mechanisms of debris flows: bed erosion, transformation from landslide, and dam
729 breach.

730 **Figure 2.** Comparison between "two-step" simulation and integrated simulation of
731 rain-induced debris flows.

732 **Figure 3.** Framework of integrated simulation of debris flows.

733 **Figure 4.** A satellite image of the study area taken shortly after the Xiaojiagou debris flow on
734 14 August 2010.

735 **Figure 5.** Rainfall process of the August 2010 rainstorm.

736 **Figure 6.** Comparison of the maximum surface runoff flow depths and flow velocities
737 simulated using FLO-2D [(a) and (b)] and EDDA 2.0 [(c) and (d)].

738 **Figure 7.** Comparison of the outflow hydrographs at the ravine mouth using FLO-2D and
739 EDDA 2.0.

740 **Figure 8.** Pore water pressure profiles at various times: (a) Case 1; (b) Case 2; (c) Case 3; (d)
741 Case 4.

742 **Figure 9.** Computed unstable cells vs. landslide scars on the satellite image.

743 **Figure 10.** Simulation results of the Xiaojiagou debris flow: (a) final shape and depth of the
744 erosion zone; (b) maximum flow velocity.

745 **Figure 11.** Comparison of the simulated and observed deposition zones: (a) simulation result;
746 (b) enlarged view of the observed deposition area (Chen and Zhang, 2015).

747 **Figure 12.** Outflow hydrograph and changes in C_v at the Xiaojiagou Ravine mouth during the
748 simulation period.

749 **Figure 13.** Distribution of C_v at different times of the storm event: (a) clear water flow; (b)
750 initiation of debris flow; (c) channelized debris flow; (d) post hyperconcentrated/clear
751 water flow.

Table 1. Parameters used in the infiltration module verification.

Case	Vertical depth (cm)	α (cm^{-1})	θ_s	θ_r	k_s (cm/h)	q_a	q_b	γ (°)	Rainfall duration (h)
1	100	0.1	0.40	0.06	10	0.1	0.9	0	20
	100				1				
2	100	0.01	0.40	0.06	1	0.1	0.9	0	20
	100				10				
3	400	0.01	0.42	0.18	3.6	0	$0.4k_{st}$	40	20
	100		0.30	0.10	0.036				
4	400	0.01	0.42	0.18	3.6	0	k_{st}	40	20
	100		0.30	0.10	0.036				

Notes: α = constitutive parameter; θ_s = saturated water content; θ_r = residual water content; k_s = saturated permeability; q_a = antecedent rainfall intensity; q_b = rainfall intensity for time greater than zero; γ = slope angle. Parameters α, θ_s and θ_r are used in the constitutive relations between the hydraulic conductivity and moisture content and the pressure head (Srivastava and Yeh, 1991).

Table 2. Properties of four types of superficial materials.

Geological type	c' (kPa)	ϕ' (°)	γ_{sat} (kN/m^3)	K_s (m/s)	α (cm^{-1})	θ_s	θ_r
Vegetated land	10.5	37	21	1×10^{-6}	0.8	0.40	0.25
Bed rock	-	-	-	0	-	-	-
Loose soil deposit	4	37	21	1×10^{-5}	0.8	0.42	0.18
Riverbed	-	-	-	1×10^{-3}	-	-	-

Notes: c' = true cohesion of soil; ϕ' = friction angle of soil; γ_{sat} = unit weight of solid particles; K_s = saturated permeability of soil.

Table 3. Soil properties for debris flow simulation.

d_{50} (mm)	ρ_s (kg/m^3)	C_{v*}	s_b	τ_c (Pa)	K_e (m^3/N-s)
35	2650	0.65	1	8.7	78.5×10^{-9}

Notes: d_{50} = mean grain size; ρ_s = density of solid particles; C_{v*} = volume fraction of solids in the erodible bed; s_b = degree of saturation of the erodible bed; τ_c = critical erosive shear stress; K_e = coefficient of erodibility.

Table 4. Constitutive (rheological) parameters for debris flow simulation.

α_1 (kPa)	β_1	α_2 (Pa·s)	β_2	K	δ_d	n
3.8	3.51	0.02	2.97	2500	0.02	0.16

Notes: α_1, β_1 = empirical coefficients for calculating τ_y; α_2, β_2 = empirical coefficients for calculating μ; K = laminar flow resistance coefficient; δ_d = deposition coefficient; n = Manning's coefficient.

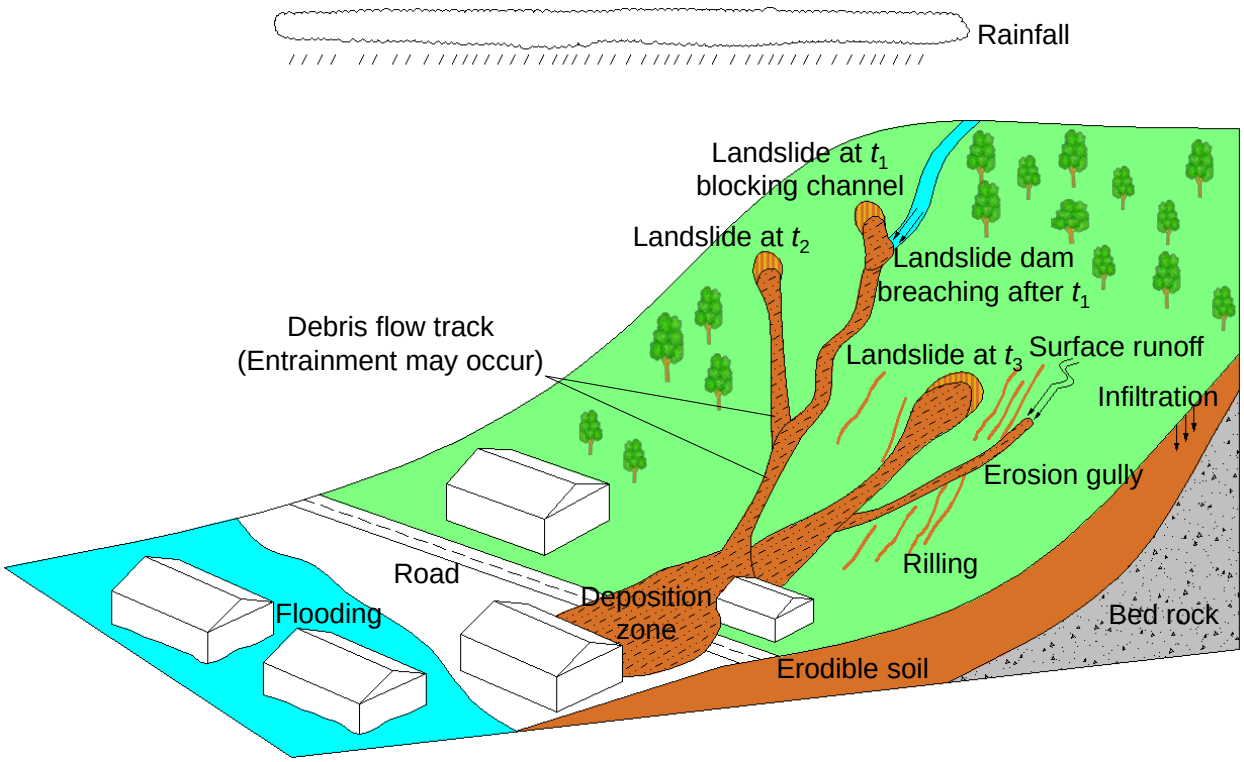

Figure 1. Conceptual model of a rain-induced debris flow and three typical initiation mechanisms of debris flows: bed erosion, transformation from landslide, and dam breach.

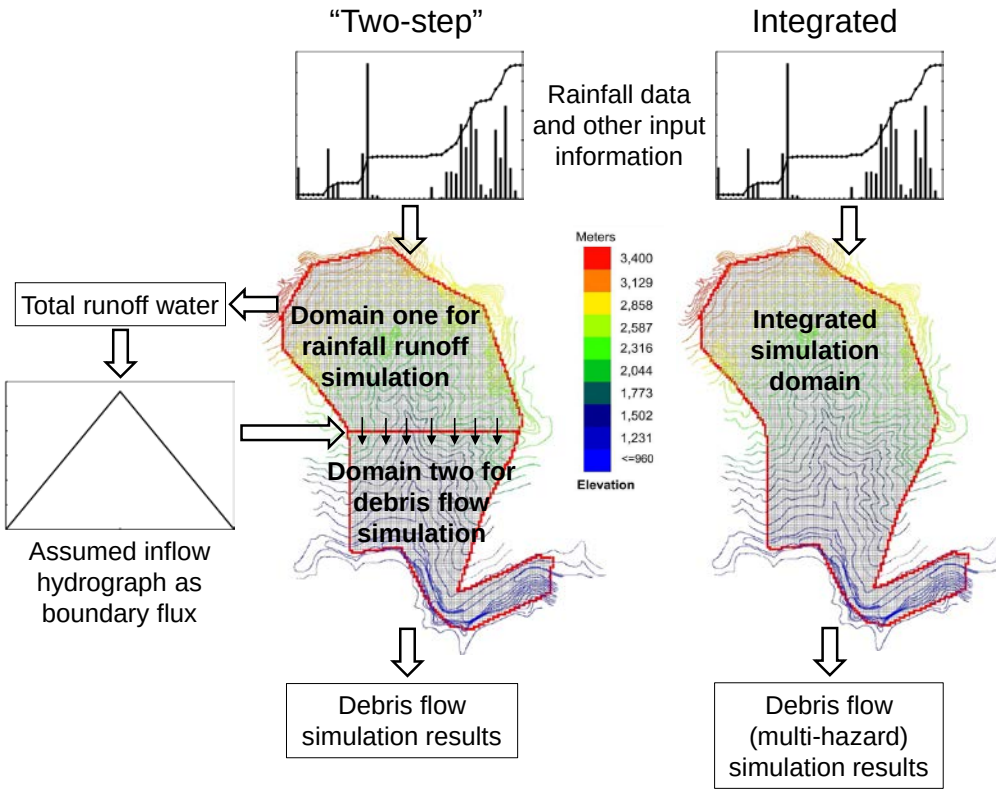

Figure 2. Comparison between "two-step" simulation and integrated simulation of rain-induced debris flows.

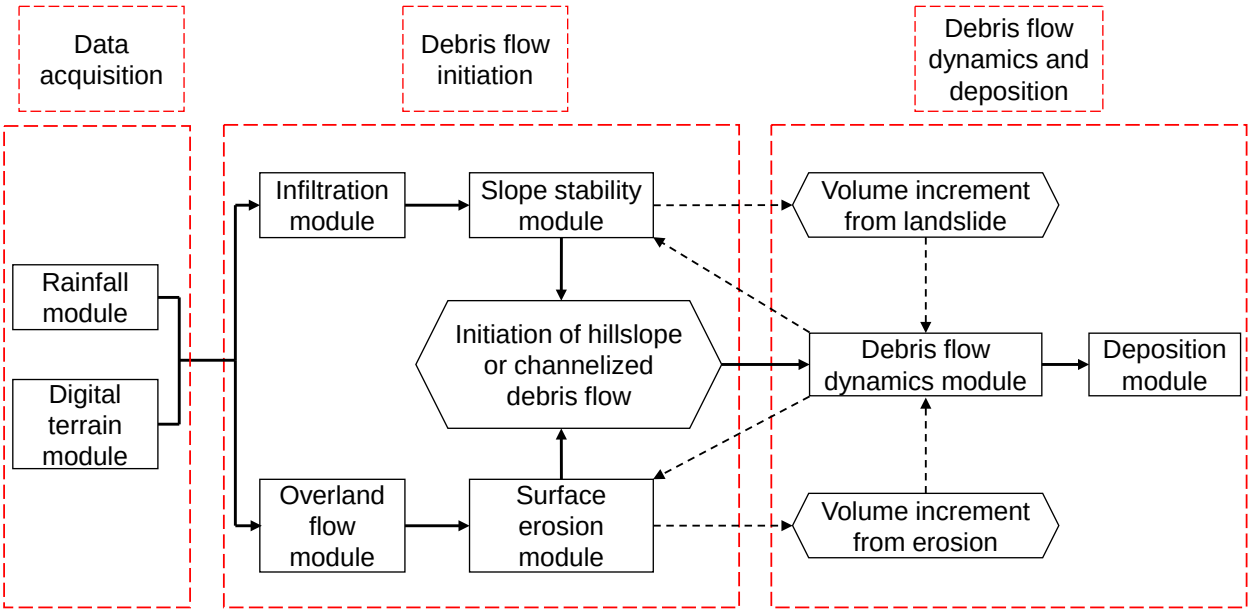

Figure 3. Framework of integrated simulation of debris flows.

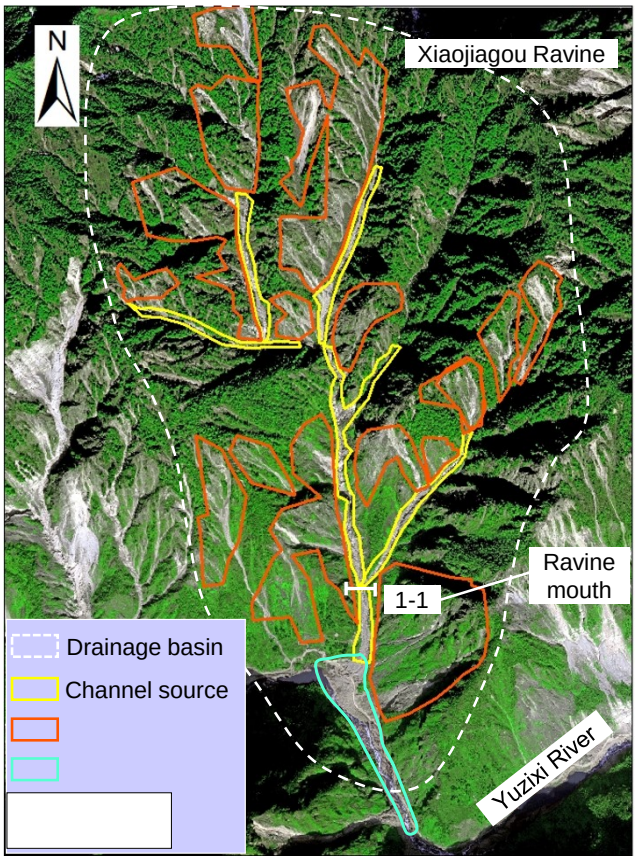

Figure 4. A satellite image of the study area taken shortly after the Xiaojiagou debris flow on 14 August 2010.

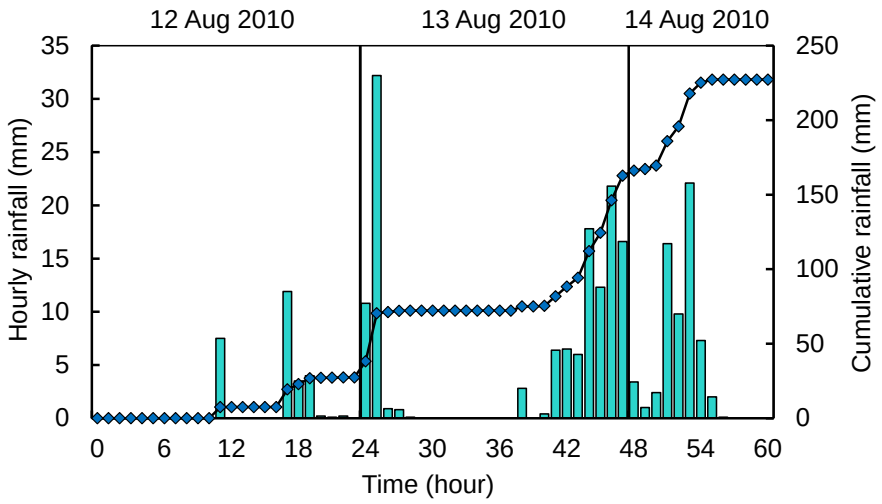

Figure 5. Rainfall process of the August 2010 rainstorm.

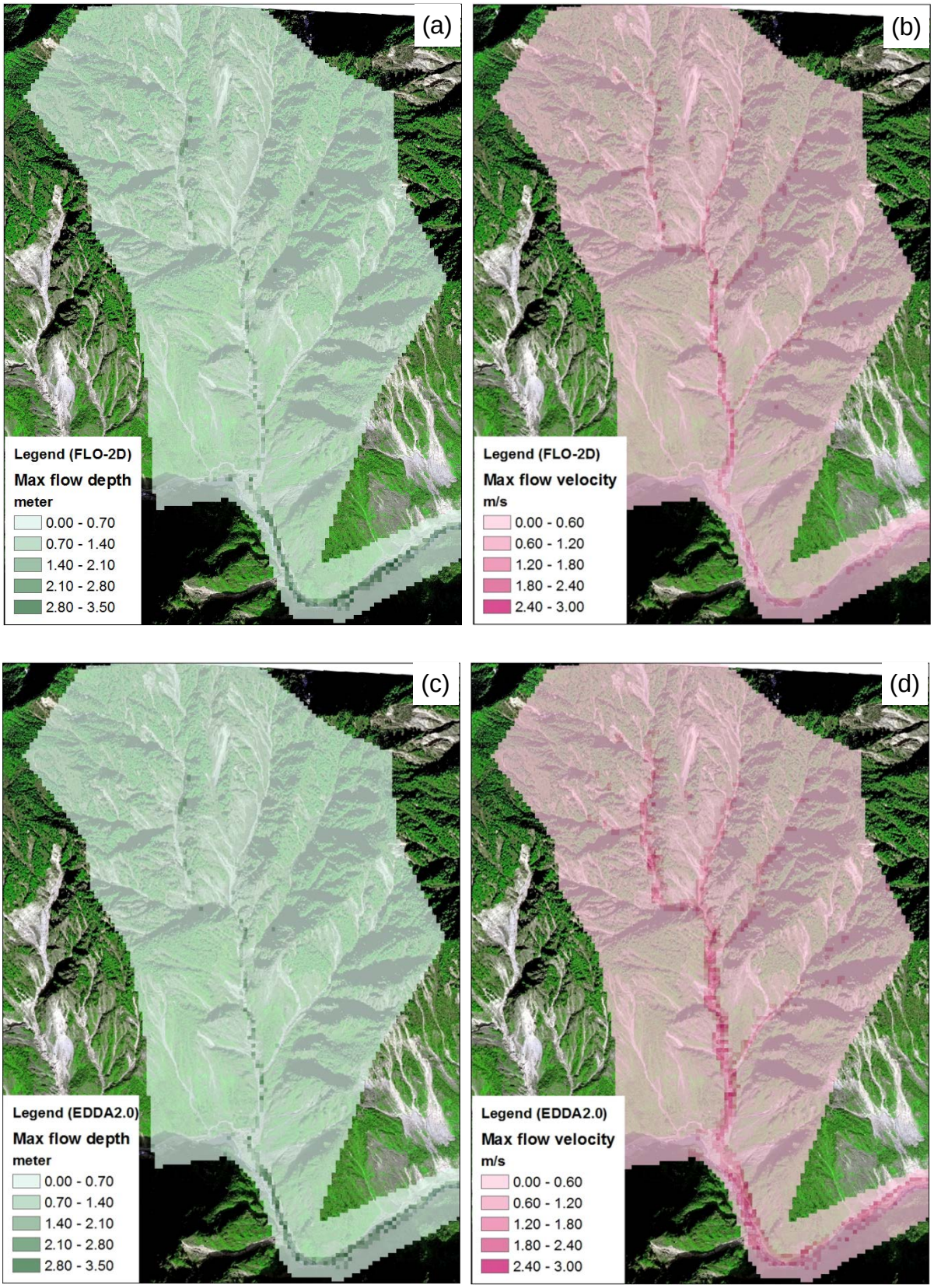

Figure 6. Comparison of the maximum surface runoff flow depths and flow velocities simulated using FLO-2D [(a) and (b)] and EDDA 2.0 [(c) and (d)].

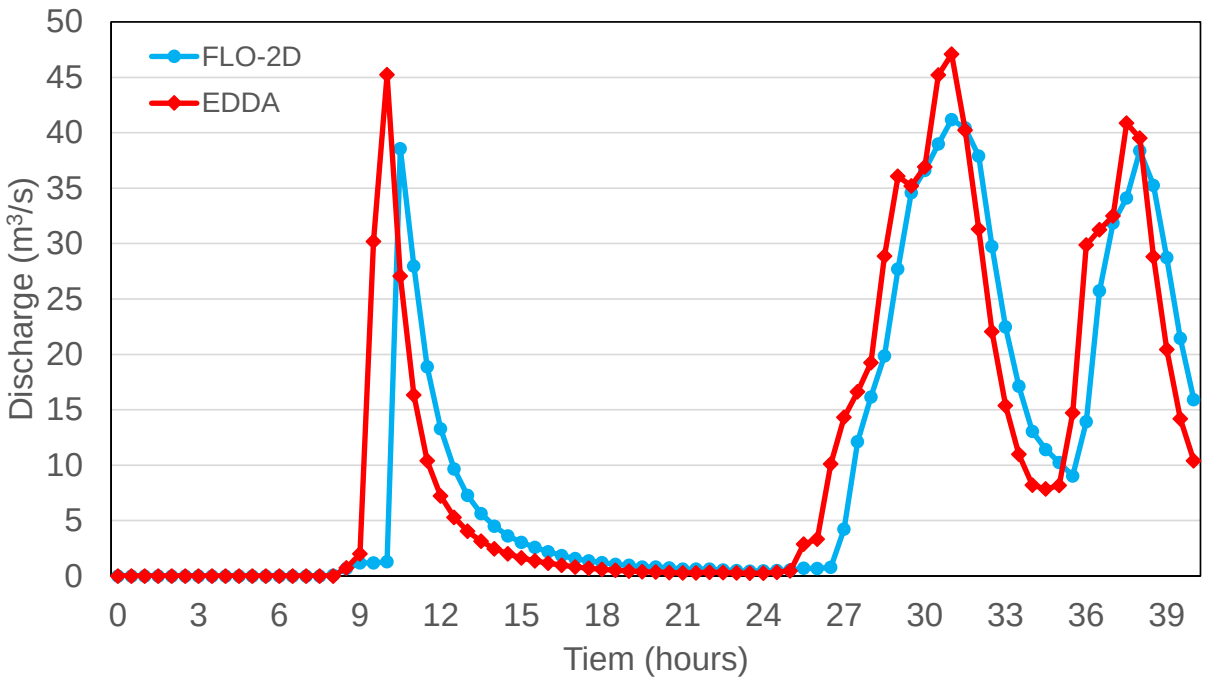

Figure 7. Comparison of the outflow hydrographs at the ravine mouth using FLO-2D and EDDA 2.0.

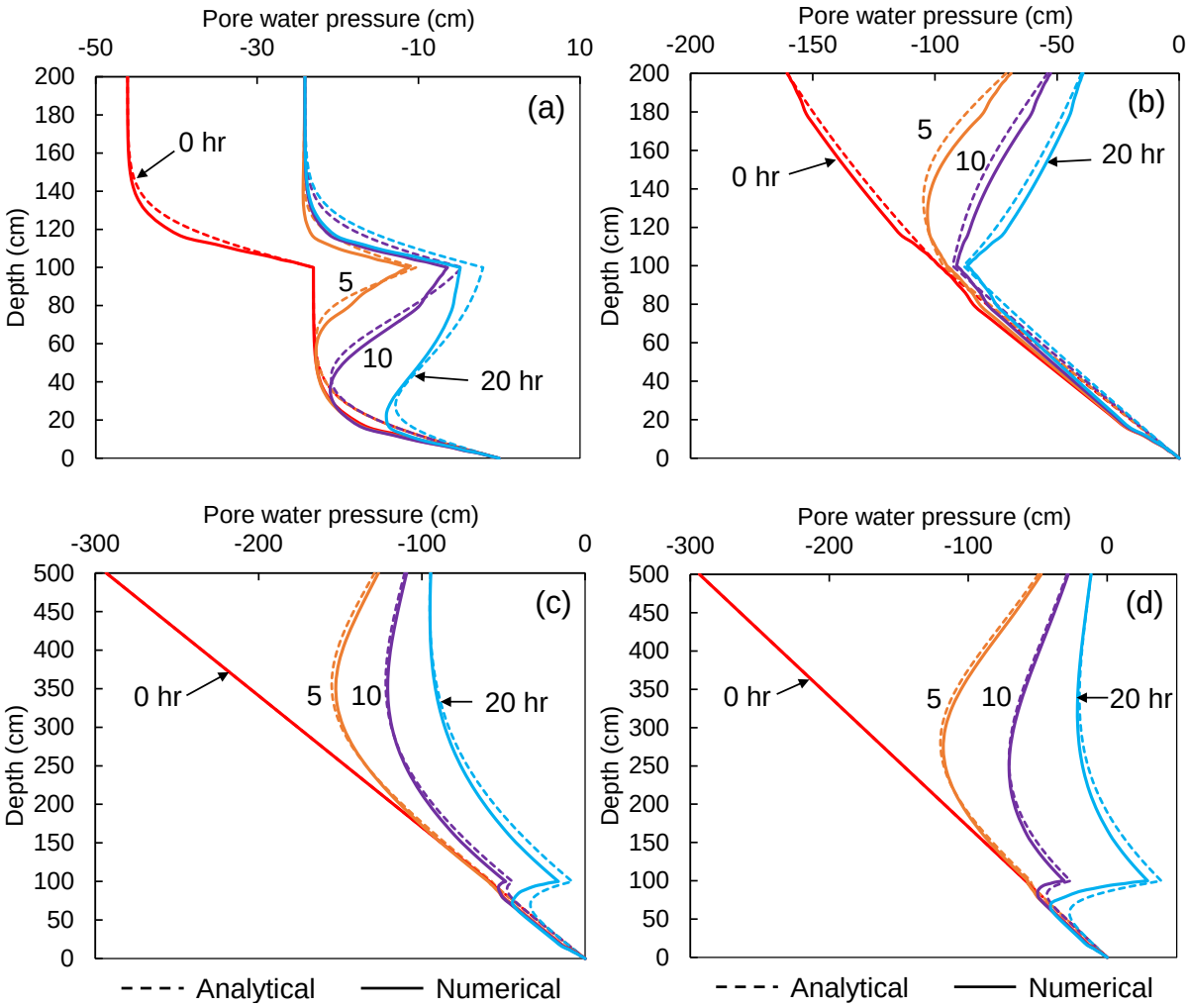

Figure 8. Pore water pressure profiles at various times: (a) Case 1; (b) Case 2; (c) Case 3; (d) Case 4.

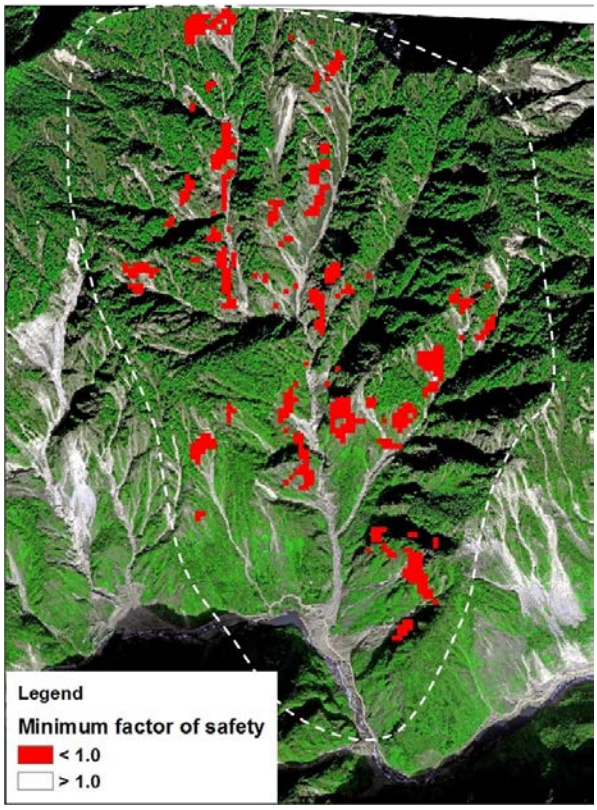

Figure 9. Computed unstable cells vs. landslide scars on the satellite image.

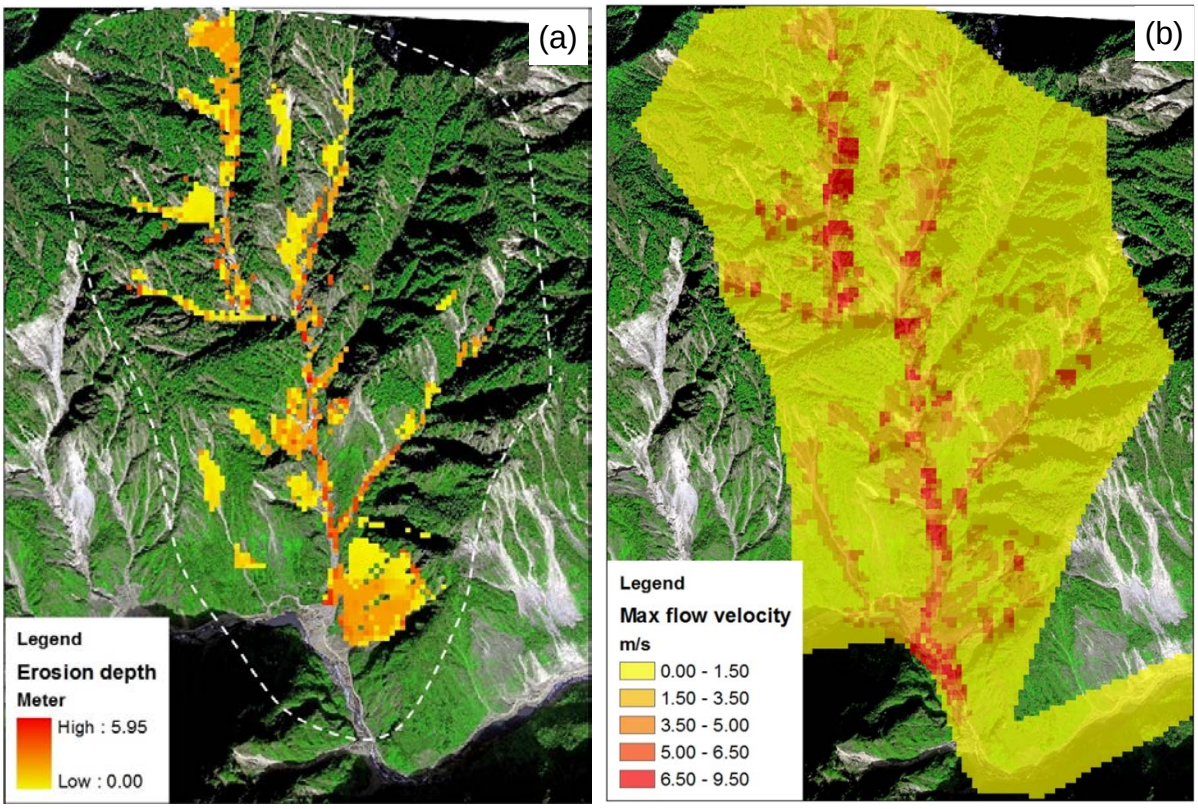

Figure 10. Simulation results of the Xiaojiagou debris flow: (a) final shape and depth of the erosion zone; (b) maximum flow velocity.

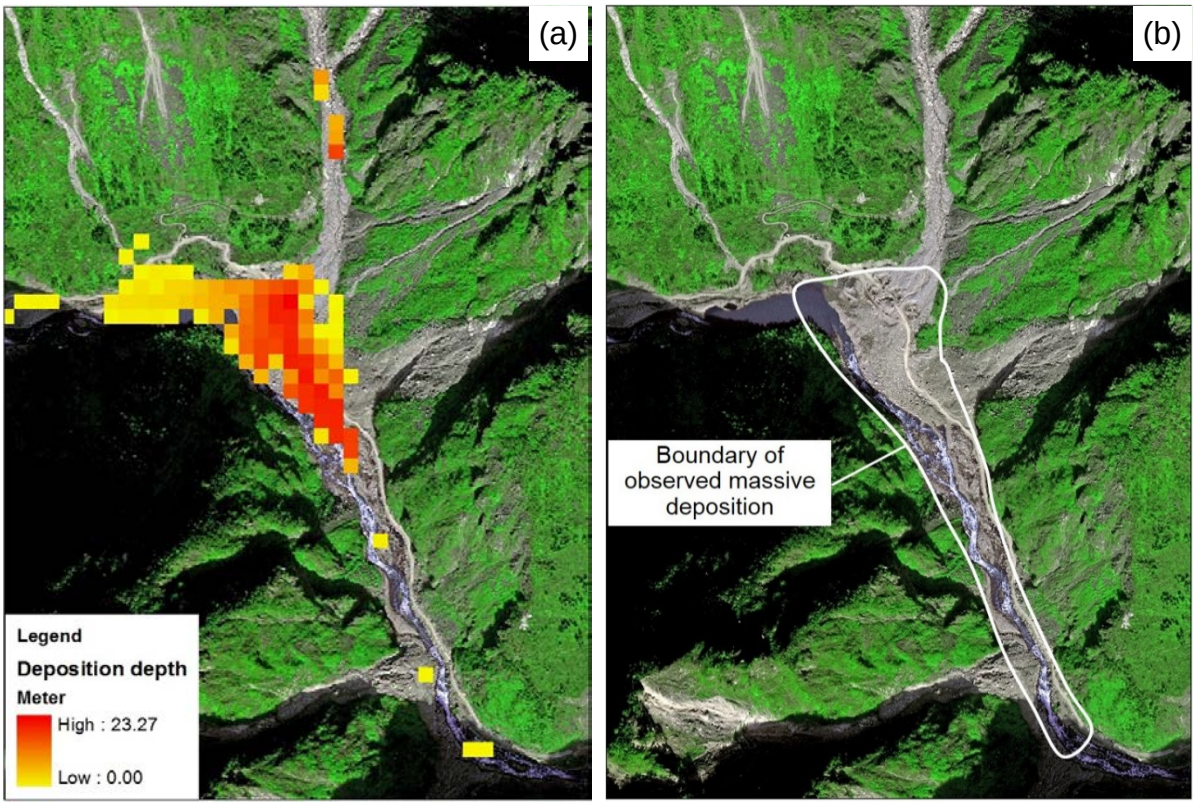

Figure 11. Comparison of the simulated and observed deposition zones: (a) simulation result; (b) enlarged view of the observed deposition area (Chen and Zhang, 2015).

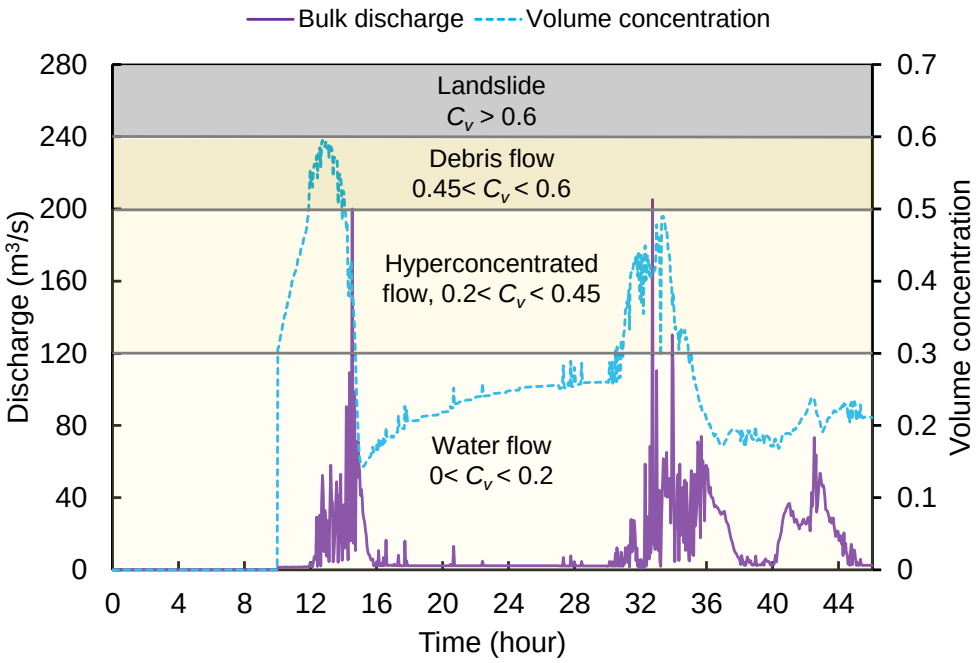

Figure 12. Outflow hydrograph and changes in C_v at the Xiaojiagou Ravine mouth during the simulation period.

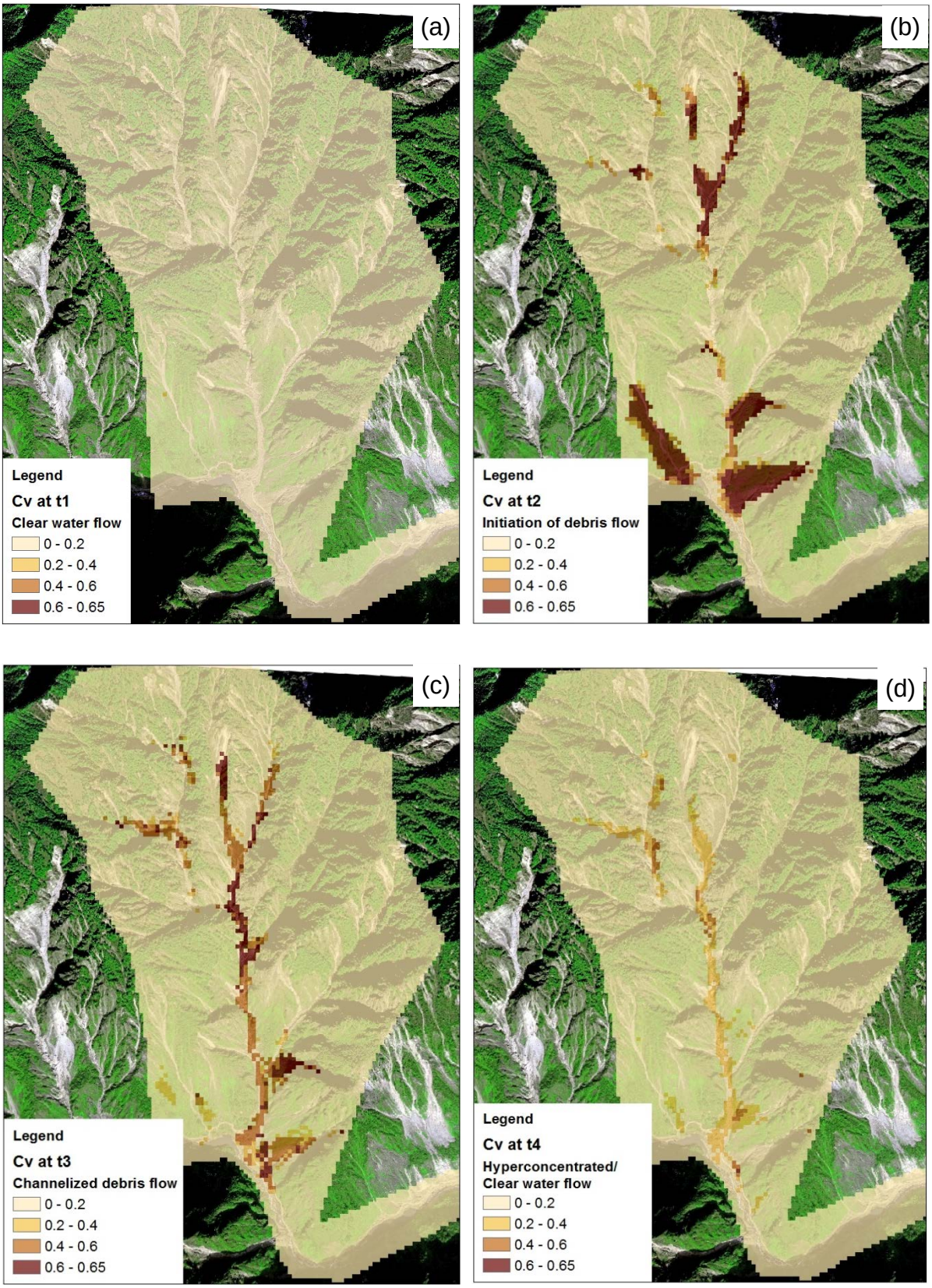

Figure 13. Distributions of C_v at different times of the storm event: (a) clear water flow; (b) initiation of debris flows; (c) channelized debris flows; (d) post hyperconcentrated/clear water flow.